Title page

Zeb2 DNA-binding sites in neuroprogenitor cells reveal autoregulation and affirm neurodevelopmental defects, including in Mowat-Wilson Syndrome.

Judith C. Birkhoff [1], Anne L. Korporaal [1], Rutger W.W. Brouwer [2], Karol Nowosad [1,3,4], Claudia Milazzo [1#], Lidia Mouratidou [1], Mirjam C.G.N. van den Hout [2], Wilfred F.J. van IJcken [1,2], Danny Huylebroeck [1,5,*], Andrea Conidi [1*, $]

[1] Department of Cell Biology, Erasmus University Medical Center, Rotterdam 3015 CN, The Netherlands; [2] Center for Biomics-Genomics, Erasmus University Medical Center, Rotterdam 3015 CN, The Netherlands; [3] Department of Biomedical Sciences, Laboratory of Molecular Genetics, Medical University of Lublin, Lublin, Poland;[4] The Postgraduate School of Molecular Medicine, Medical University of Warsaw, Warsaw, Poland; [5] Department of Development and Regeneration, KU Leuven, Leuven 3000, Belgium

* *shared senior authors*

[#] *Present address*: Dept. Clinical Genetics, Erasmus University Medical Center, Rotterdam, 3015 CN, The Netherlands

[$] *Lead author for correspondence*:

Andrea Conidi, Dept. Cell Biology, Erasmus MC, Building Ee - room Ee-1040, Wytemaweg 80, 3015 CN Rotterdam, The Netherlands;

Tel: +31-10-7043169; Fax: +31-10-7044743; E-mail: a.conidi@erasmusmc.nl

Abstract

Perturbation and mechanistic studies have shown that the DNA-binding transcription factor Zeb2 controls cell fate decision and differentiation and/or maturation in multiple cell lineages in embryos and after birth. In cultured embryonic stem cells (ESCs) *Zeb2*'s strong upregulation is necessary for the exit from primed pluripotency and for entering general and neural differentiation. We edited mouse ESCs to produce epitope-tagged Zeb2 from one of its two endogenous alleles. Using ChIP-sequencing, we mapped 2,432 DNA-binding sites of Zeb2 in ESC-derived neuroprogenitor cells (NPCs). A new, major site maps promoter-proximal to *Zeb2* itself, and its homozygous removal demonstrates that *Zeb2* autoregulation is necessary to elicit proper Zeb2-dependent effects in NPC differentiation. We then cross-referenced all Zeb2 DNA-binding sites with transcriptome data from Zeb2 perturbations in ESCs, ventral forebrain in mouse embryos, and adult neurogenesis from the mouse forebrain V-SVZ. While the characteristics of these neurodevelopmental systems differ, we still find interesting overlaps. This contributes to explaining neurodevelopmental disorders caused by *ZEB2* deficiency, including Mowat-Wilson Syndrome.

Introduction

Zeb2 (also named Sip1/Zfhx1b) and Zeb1 (δEF1/Zfhx1a), the two members of the small family of Zeb transcription factors (TFs) in vertebrates, bind to two separated CACCT (often also to CACCTG E2-boxes) and sometimes CACANNT(G) sequences on DNA via two (between Zeb1 and Zeb2) highly conserved, separated clusters of zinc fingers (1-4). Mutations in *ZEB2* cause Mowat-Wilson Syndrome (MOWS, OMIM#235730) (5-7), a rare congenital disease displaying intellectual disability, epilepsy/seizures, typical facial dimorphism, and often Hirschsprung disease, and multiple other defects in the patients (8-10). Typical are also the delay in developmental milestones and motoric development, and eye and tooth anomalies. Other features are specific craniofacial malformation, sensorineural deafness, and HSCR, which originate from defects in the ZEB2-positive (+) cells of the embryonic neural crest cell lineage. Mutant *ZEB2* alleles have meanwhile been determined for about 350 patients (11-16). Reports have described malformations in the central nervous system (CNS) of MOWS patients over broad age range, in which the observed defects locate to the corpus callosum and/or hippocampus, and can be seen by neuroimaging and follow-up of electro-clinical defects, which include focal seizures (16-18).

Zeb2's action mechanisms, partner proteins, few proven or candidate direct target genes, and genes whose normal expression depends on intact Zeb2 levels, have been studied in various cell types, explaining specific phenotypes caused by Zeb2 perturbation. Zeb2 DNA-binding around candidate

direct target genes helped to explain *Zeb2* loss-of-function phenotypes in ESCs and cells of early and late embryos, and in postnatal and adult mice. These genes are involved in ESC pluripotency (*Nanog*, *Sox2*), cell differentiation (*Id1*, *Smad7*), and maturation of various cell types, e.g., in embryonic cortical and adult neurogenesis (*Ntf3*, *Sox6*), as well as epithelial-to-mesenchymal transition (EMT) (*Cdh1*) (19-26). In reverse, subtle mutagenesis of Zeb2 DNA-binding sites in demonstrated target genes has confirmed Zeb DNA-binding and its repressive activity (e.g., on mesodermal X*Bra* (27) and epithelial *Cdh1* (19)).

Despite its critical function in the precise spatial-temporal regulation of expression of system/process-specific relevant genes during embryogenesis and postnatal development, but recently also adult tissue homeostasis and stem cell-based repair, and acute and chronic disease (28, 29; for a recent review, see (30)), ChIP-sequencing (ChIP-seq) data for Zeb2 has been obtained in very few cases only. A major reason is that ChIP-seq grade antibodies specific for Zeb2 are not readily available. Data have been published for high-Zeb2 hepatocellular carcinoma and leukemia cell lines, or cultured cells that overproduce tag-Zeb2 from episomal vectors or the safe *Rosa26* locus (25, 31, 32), neither of which represent endogenous Zeb2 levels nor express *Zeb2* with normal dynamics. Furthermore, most, if not all, anti-Zeb2 antibodies cross-react with Zeb1, so do not discriminate between both proteins when their presence overlaps or succeeds to one another. However, they compete for the same target genes, which for the individual proteins depends on cell identity/state, extrinsic stimulation or cellular context (e.g., in somitogenesis (33) and melanoma (34)).

During neural differentiation (ND) of mouse (m) ESCs, Zeb2 mRNA/protein is undetectable in undifferentiated cells, whereas its strong upregulation accompanies efficient conversion of naïve ESCs into epiblast stem cell like cells (EpiLSCs) and is essential for subsequent exit from primed cells and onset of differentiation, including progression to neuroprogenitor cells (NPCs) (25). We have edited one *Zeb2* allele of mESCs by inserting a Flag-V5 epitope tag (in brief, V5) just before the stop codon, in-frame with the last exon (ex9 of mouse *Zeb2*, (35)). Such Zeb2-V5 mESCs were then differentiated to NPCs, and Zeb2 binding sites were determined by V5-tag ChIP-seq. Doing so, we identified 2,432 binding sites, 2,294 of which map to 1,952 protein-encoding genes. We then cross-referenced the ChIP+ protein-encoding target genes with RNA-seq data of deregulated expressed genes (DEGs) in cell-type specific neurodevelopment-relevant Zeb2 perturbations (23, 36, 37). Although we compare non-identical systems, the overall approach still revealed a number of interesting overlaps, as well as Zeb2's role in regulating critical targets in neurodevelopment. Taken together, we report for the first time the identification of endogenous genome-wide binding sites (GWBS) in ESC-derived neural cells for the MOWS TF ZEB2.

Results

Heterozygous Zeb2-V5 ESCs differentiate as wild-type cells

Addition of short epitope(s) at the N- or C-terminus, as well as activation/repression domains of heterologous TFs at the Zeb2 C-terminus, does not interfere with Zeb2's DNA-binding (as tested in *Xenopus* embryos (38), heterologous cells (39), mouse forebrain (36) and mESCs (25)). Here, we have used a CRISPR/Cas9 approach (see Materials & Methods) to insert an in-frame Flag-V5-tag encoding sequence in *Zeb2*-ex9 of mESCs (clone 2BE3; Fig. S1). Allele-specific RT-qPCR using primers that amplify sequences between the ex9 and the V5-tag showed mRNA expression from the tagged allele during ND in cell culture at day (D) 0, 4, 6 and 8 (Fig. 1A). Western blot analysis in nuclear extracts of ND-ESCs at D8, thus in NPCs (25), confirmed the presence of Zeb2 of expected relative molecular mass, using either anti-V5 (αV5) or anti-Zeb2 antibodies (Fig. 1B). Both the Zeb2-V5 and wild-type ESCs were then also verified during ND differentiation for temporal expression of *Zeb2*, core pluripotency genes (*Pou5f1*, *Nanog*, both downregulated upon ND, and *Sox2*, also a NPC TF) and an acknowledged NPC marker (*Pax6)* (Fig. 1C,D).

Both cell lines displayed comparable expression dynamics of these genes, indicating that Zeb2-V5 NPCs at D8 of ND can be used for ChIP-seq. Further confirmation came from selective pull-down of Zeb2 on the known target *Cdh1*, using ChIP-qPCR. Zeb2 binds to 2 of 3 E-boxes in the mouse *Cdh1* promoter (Fig. 1E), which it represses during EMT (19, 25). A ±25-fold enrichment for Zeb2-V5 was obtained when probing this *Cdh1* region using anti-V5 antibody (αV5) conjugated beads compared to agarose beads as negative control (Fig. 1F). Hence, the Zeb2-V5 protein binds to known Zeb2 target sites, and the NPCs are suitable for endogenous mapping of the Zeb2 GWBS.

One-third of 2,432 Zeb2 DNA-binding sites map close to the transcription start site of transcriptome-confirmed, system-relevant protein-encoding genes, including *Zeb2* itself

αV5-precipitated samples from upscaled Zeb2-V5 NPCs were used for cross-link ChIP-seq, followed by analysis with Galaxy Software (see Materials and Methods; 40). Of the total of 2,432 significant peaks, 2,294 peaks (94% of total) mapped to 1,952 loci that encode protein, while 125 peaks (5% of total) map to micro-RNA (miRNA) genes, and 1% to regions lacking annotation (NA, using ENSEMBL-GRCm38.99; Fig. 2A; File S1). In addition, about 37.5% of all binding sites of Zeb2-V5 are located within -10/+10 kb of annotated transcription start sites (TSS, Fig. 2B). Gene ontology (GO) pathway enrichment analysis of the aforementioned 1,952 loci revealed binding of Zeb2 to

classes of genes annotated to Wnt, integrin, chemokine/cytokine (predominantly as defined in inflammation) and cadherin signaling, respectively, as well as to developmental signaling by EGF, VEGF, TGFβ and FGF family pathways (Fig. 2C). Among these 1,952 loci, those for genes encoding transcription regulatory proteins, and post-translational modification as well as metabolic enzymes are well-represented (Fig. 2D).

In parallel we applied bulk temporal RNA-seq of wild-type mESCs at D0 (undifferentiated), D4 (neural induction), D6 (early NPCs) and D8 (NPCs) and checked the expression dynamics of the 1,952 Zeb2-bound genes (from the D8 sample). Among these, 1,244 were subject to significant transcriptional regulation between D4-8 as compared to D0 (Fig. 2E; log2FoldChange <-0.5 or >0.5 and p-value < 0.05; low-stringency analysis was opted to assess also small differences in mRNA of Zeb2-bound genes). Further, 335 of these genes are commonly expressed between D4-6-8, but at different levels, including *Zeb2* itself (for lists of all DEGs, see File S2). Fig. S2A depicts the D4, D6 and D8 transcriptomes of ND-mESCs, each compared to D0, with indication whether the genes are bound or not by Zeb2, as determined by Zeb2-V5 ChIP-seq. At each of these respective time points, hence at different Zeb2 mRNA level, about 12% of the DEGs are bound by Zeb2 (Fig. S2B).

Among the Zeb2-bound genes that normally become down-regulated, *Dnmt3l* and *Esrrb* are present, suggesting that upregulation of *Zeb2* in ND-ESCs (D6 and D8) directly causes downregulation of these two genes accordingly (Fig. S2C; File S2). Zeb2 has been suggested as direct repressor of *Dnmt3l* and *Esrrb*, facilitating the switch from self-renewal of ESCs to their exit from pluripotency, and promoting differentiation. Indeed, expression levels of all *Dnmt3* genes remained higher in *Zeb2*-knockout (KO) ND-ESCs (25). However, these *Zeb2*-KO cells also convert very inefficiently into EpiLSCs and fail to exit from primed pluripotency. Importantly, among the Zeb2-binding genes whose mRNA levels increased during ND, *Zeb2* itself is also present (yellow dot, Fig. S2C), indicating autoregulation. In fact, in this ND model the highest recruitment of Zeb2-V5 in ChIP-seq data was mapped upstream the TSS of *Zeb2* (File S1).

Out of the 1,244 Zeb2-bound genes that significantly changed steady-state mRNA levels in our D4 to D8 transcriptome data sets, 213 are exclusive DEGs in NPCs at D8 (Fig. 2E; Fig. S2D). Among these, *Tcf4* is bound by Zeb2 and becomes highly upregulated in NPCs (Fig. 2E; Fig. S2D). Tcf4 is a ubiquitous basic helix-loop-helix (bHLH) type TF that binds to E-boxes, and co-operates in many isoforms (41, 42) with cell-type specific bHLH TFs as heterodimers, which are active during CNS development ((43, 44); for a review, see (45)). In oligodendrocyte precursors (OPCs), Tcf4 is essential for their subsequent differentiation. It dimerizes with the lineage-specific bHLH-TF Olig2, further promoting their differentiation and maturation (46), while Zeb2 together with upstream Olig1/2 are essential for myelinogenesis in the embryonic CNS (21). Here, Zeb2 generates anti-BMP(-Smad)/anti-Wnt(-β-catenin) activities, which is crucial for embryonic CNS myelinogenesis emanating from differentiation of OPCs. The regulatory action of Zeb2 on the *Tcf4* target gene, as found in mouse cells by our ChIP-seq, may underpin phenotypic similarities between MOWS and Pitt-Hopkins syndrome

patients (PTHS, OMIM #610954), the latter caused by mutations in *TCF4* (47), making us speculate that *TCF4* may be deregulated in MOWS neural cells.

Zeb2 peaks overlap with active enhancers and promoters within -10/+10 kb from the TSS

To assess whether Zeb2-peaks are present in the regulatory regions of up- or down-regulated genes from our transcriptome data, we cross-referenced the coordinates of the Zeb2 broad peaks within -10/+10kb from the TSS, with the mouse ChIP-seq datasets available in ENCODE for neuronal tissues (cerebellum, cortical plate, olfactory bulb, forebrain, midbrain, hindbrain, neural tubeolfactory bulb). We found that of the different histones ChIP-seq datasets available in ENCODE H3K27ac, H3K4me1 and H3K4me3 marks were overlapping with our ChIP-seq data (Figure 2F). The H3K27ac signature strongly overlaps with the Zeb2 peaks in genes upregulated at D8 (19% in upregulated genes vs. 4% in downregulated genes). For H3K4me1 and H4K4me3 marks, no big difference in overlap between up- and down-regulated genes was observed. While H3K27ac mark is associated with active enhancers, H3K4me1 is associated with primed enhancers, and H3K4me3 is considered a "promoter" marker (48). Taken together these data suggest an activating role for Zeb2 at this stage of differentiation. Outside the -10/+10kb considered range, about 48% of the identified peaks overlap for about 48% with H3K27Ac and 52% with H3K4me1 histone marks (Fig. 2G).

We then performed motif enrichment analysis using UniBind (https://unibind.uio.no) for TFs that could bind the Zeb2-bound peaks and in proximity of up- or down-regulated genes at D8 of mESCs differentiation (S3A and B). In those peaks close to the TSS of upregulated genes, motifs for Sox2, Gata2 and Tcf3 are very abundant. These TFs are known to have a function during NPC or neural differentiation. Sox2 is an acknowledged marker for neurogenesis (49) and during later stages of differentiation. It has been demonstrated that Zeb2 exhibit anti-Sox2 activities in myelination and re-myelination by adult Schwann cells in the PNS, needed for normal progression of commitment, differentiation and maturation in this glial cell lineage (21, 24, 29,50). Tcf3 (also named E2A) plays a role in stem cell self-renewal (51), but is also important during neural fate commitment and possibly repressing Nodal signaling during neural differentiation (52). Gata2 has been associated with negatively regulating proliferation in NPCs and, by doing so, directing these cells further into differentiation (53). However, how Zeb2 acts upon, or together with these TFs during NPC differentiation. is not fully worked-out yet.

In the peaks close to the TSS of downregulated genes there is a prevalence for CTCF, Fos, Myc and Stat5a binding. CTCF is likely of specific interest for its moieties to act as a link between 3D genome architecture to gene regulation. During NPC differentiation however, it was observed that 40% of the NPC-specific DNA-loops were not CTCF-dependent, whereas in other cell-state specific loops, this was only 10%, indicating a less important role for CTCF in the regulation of NPC

differentiation compared to differentiation into other cell lineages (54). This might indicate an interesting role for Zeb2 in repressing CTCF levels during NPC differentiation, supporting the subsequent activation of NPC-specific genes. Also here, more studies are required to get more insights into the co-operativity or counteracting actions of Zeb2 with candidate TFs in the regulation of the candidate Zeb2 targets.

Meta-analysis of RNA-seq data from selected neural-system *Zeb2* perturbations and the NPC ChIP-seq data reveal interesting overlaps

We performed a meta-analysis of three published transcriptome data sets from control and *Zeb2*-KO mice: sorted E14.5 mouse ventral forebrain interneurons (Nkx2.1-Cre driven *Zeb2*-KO; (36)) and sorted (at P2) progenitors of the V-SVZ, an adult neurogenic niche (Gsh2-Cre; 36). In addition, we used high-throughput RT-qPCR data generated on a Fluidigm platform and obtained after esiRNA-based knockdown (KD) of Zeb2, as part of a systems-biology study in ND-mESCs ((37) (the Zeb2 KD data subset was kindly provided by R. Dries). From these respective datasets, the DEGs upon the Zeb2 perturbations (p-value <0.05; log2FoldChange<-1 and >1) were filtered. This identified (i) genes that depend on normal Zeb2 levels for their downregulation/repression (if directly by Zeb2, as repressor) or (ii) other genes that depend on Zeb2 for their upregulation/activation (if directly by Zeb2, as activator) (for Zeb2 as dual TF, see (29); (30, 55)). In parallel, our 2,294 Zeb2-V5 sites mapping to the 1,952 protein-encoding genes were filtered from the complete ChIP-seq dataset, and then used as reference for the RNA data sets (Fig. 3A).

This cross-referencing identified 108 protein-encoding genes among the three transcriptomic data sets and ChIP-seq data set (Fig. 3A). Fig. S4 shows a heatmap of the changes in mRNA levels of these 108 genes during ND of wild-type ESCs and their correlation with the analyzed datasets. Noteworthy, only *Cxcr4* was common to all RNA data sets. This is likely due to the fact that two RNA-seq sets are generated in different brain/neuron cell-type *in vivo* mouse models, while the other steady-state RNA level data documented the effects of Zeb2-KD on mRNA levels of (only 96 in total) TGFβ/BMP-system components (37), so the timing does not completely overlap with our ChIP-seq dataset. However, Cxcr4 and its ligand Cxcl12/Sdf-1 are crucial for migration of interneurons from the ventral forebrain to the neocortex (56, 57), processes co-controlled by Zeb2 as shown in cell-type specific KO mice (36). Furthermore, the identified 108 genes are involved in regulation of stem cell pluripotency, signaling by TGFβ, FoxO, and Hippo, and in axon guidance. Taken together these data further confirms the pivotal role of Zeb2 in these processes.

Zeb2 directly controls TGFβ/BMP-system component and neuronal differentiation/ migration genes

We then validated 14 out of the 108 cross-referenced target genes, selected based on either being already known as a target of Zeb2 (*Nanog*), or as TGFβ/BMP-system component (*Bmp7, Tgfbr2, Smad1, Smad2, Smad3, Id2, Cited2*), or having a crucial role in neurogenesis and neuronal maturation (*Sema3f, Cxcr4, Lhx5, Ntng2, Pax6, Tcf4*; their mRNA levels in ND-ESCs are highlighted in the heatmap in Fig. S4). Because *Zeb2*-KO ESCs do not exit from primed pluripotency and thus cannot differentiate (25), we chose to validate our findings using shRNA-mediated Zeb2-KD at ND-D8, and analyzed these aforementioned 14 genes two days later (at D10 NPCs) (Fig. 4A); at this read-out time point >50% reduction of Zeb2 mRNA was obtained (Fig. 4B).

Zeb2-KD resulted in reduced mRNA levels of *Cxcr4*, *Ntng2* and *Pax6* (Fig. 4B), genes that are each involved in neuron specification and migration (58, 59). Zeb2-KD also caused down-regulation of *Lhx5*, involved in differentiation of interneurons, including cytoskeletal rearrangements during dendritogenesis (60), and of *Tcf4*, which acts in neurogenesis (43, 44). *Sema3f is a* cue for axon outgrowth and neuron migration guidance, and was slightly upregulated (Fig. 4B). These results confirm the regulation by Zeb2 of its direct targets in later phases of neuronal differentiation/migration.

The expression of *Nanog*, the promoter of which binds Zeb2 as a repressor (25), was increased in the Zeb2-KD cells (Fig. 4B). Zeb2-KD caused increased mRNA of *Bmp7, Tgfbr2, Smad1, Smad2, Smad3* and *Cited2* (Fig. 4B), fitting with the normal levels of Zeb2 that mount anti-TGFβ/BMP family effects (29). In contrast, *Id2* is significantly downregulated in shZeb2-treated ESCs (Fig. 4B). *Id2* is normally activated by BMP-Smads and, together with other Id proteins (Id1, Id3 and Id4), inhibits cell differentiation, e.g., Zeb2 represses *Id2* in immune cells to promote differentiation (22). However, *Id2* as well as other *Id* genes (61-63) is, like *Zeb2* (20, 36), also expressed in the developing forebrain. Taken together, these data suggest an active and direct role for Zeb2 in repressing genes regulating stem cell pluripotency as well as a number of TGFβ/BMP-system components (*Bmp7*, *Smad1/2/3*), but also in activating genes during neurogenesis (*Cxcr4, Ntng2, Lhx5*).

Zeb2 potentiates its own gene expression, which is crucial for proper control of some of its direct target genes

Strikingly, in our ChIP-seq dataset, the peak with the highest enrichment (~200-fold) mapped 232 bp upstream of the Zeb2 TSS (Fig. 5A, File S1). For further functional studies of this site, we deleted the encompassing region (chr2:45109746-45110421) using CRISPR/Cas9 in wild-type mESCs, thereby obtaining *Zeb2*$^{\Delta P/\Delta P}$ ESCs (Fig. S6; see Materials and Methods). Fig. 5B shows that the Zeb2 mRNA

levels in the homozygous *ΔP* clone stayed significantly low during ND, already from D8 onwards, compared to control cells, classifying this *Zeb2*$^{\Delta P/\Delta P}$ clone as an alternative Zeb2-KD.

We then used these *Zeb2*$^{\Delta P/\Delta P}$ mESCs to read-out the same genes that depend on intact Zeb2 levels and are Zeb2 ChIP+ (see Fig. 4B). Levels of Zeb2 mRNA stayed abnormally very low at D10 in *Zeb2*$^{\Delta P/\Delta P}$ ND-mESCs, whereas *Nanog* was still expressed and remained higher than in control WT cells (Fig. 5B). Hence, Zeb2 levels, including those achieved by autoregulation, are critical, but to a different degree for sets of genes. The latter include neuronal-relevant genes such as *Cxcr4*, *Lhx5*, *Ntng2*, *Pax6*, *Tcf4* (Fig. 5B). Among the TGFβ/BMP-system components (see Fig. 4) we observed a slight reduction of *Bmp7*, *Smad1* and *Smad3*, whereas *Tgfbr2*, *Smad2*, *Cited2* and *Sema3f* expression was not affected in *Zeb2*$^{\Delta P/\Delta P}$ ND-mESCs. We speculate that Zeb2, and now including its newly identified autoregulation, plays an active role in regulating a number of genes involved in neuron determination and, together with other TFs, TGFβ/BMP-system component genes. Thus, the precise amounts of Zeb2, and in a critical stage also its autoregulation, are crucial in discriminating genes where Zeb2 plays the aforementioned primary, active role (as for *Cxcr4*, *Lhx5*, *Ntng*2 etc.). For these genes, ~50% reduction or the novel *ΔP/ΔP* "peak" mutation is sufficient to strongly deregulate them, but other genes' expression is either not or just slightly affected (*Sema3f*, *Smad2*, *Cited2* vs. *Bmp7*, *Tgfbr2*, *Smad1*, *Smad3*).

Because Zeb2 also binds phospho(p)-Smads (4, 21, 23, 29), we also scanned the Zeb2 ChIP+ direct target genes, and for which we saw strong deregulation upon Zeb2-KD and/or in *Zeb2*$^{\Delta P/\Delta P}$ cells during ND (wherein notably Smad-activation is not stimulated), for the presence of (i) the Zeb half-sites CACCT(G) (pragmatically neglecting the variable spacing between them; 64) that combine with (ii) candidate p-Smad binding and responsive genes (using GTC($^{T}/_{G}$)CT($^{T}/_{G}$)($^{A}/_{C}$)GCC for p-Smad1/Smad5, GTCTAGAC for p-Smad2/3) and (iii) the co-Smad Smad4 (C($^{C}/_{T}$)AGAC) (65), using the Jaspar database. Fig. S6 shows the distribution of such identified Zeb and Smad-binding motifs (threshold score >85%) in those genes strongly affected by Zeb2-KD and/or in *Zeb2*$^{\Delta P/\Delta P}$ cells. Interestingly, in the regions where Zeb2 binds close to the TSS (*Zeb2*, *Ntng2*, *Lhx5*, *Nanog*), the p-Smad and Smad4 binding elements are sometimes present in very close proximity of the ChIP+ Zeb2-bound E-box, indicating a possible cross-talk between receptor-activated Smads and Zeb2 in regulating target genes.

Discussion

We report for the first time the endogenous GWBS for Zeb2 by ChIP-seq, in ESC-derived NPCs gene-edited for this. We have previously used ESCs established from *Zeb2*$^{\Delta ex7/\Delta ex7}$-KO (66) pre-implantation embryos and, for rescue purposes, such KO ESCs cells in which $Flag_3$-Strep-Zeb2 was produced from

(a Cre-controllable) *Rosa26* locus (25). Conceptually, with regard to Zeb2 levels, the latter cells are different from the mESCs that were newly established here, since in the original Rosa26-Zeb2 cells *Zeb2* is not subjected to its normal temporal regulation during cell differentiation.

However, precise dosage of Zeb2 is a critical factor *in vivo* (for a recent discussion, see 30). This is concluded from transgenic Zeb2 cDNA-based rescues in *Zeb2*-KO ESCs and similar genetic rescues in *Zeb2*-mutant cells in mice, which can via heterozygous/homozygous combinations create an elegant and large panel of Zeb2 levels (in interneurons (36), NK cells (67), ESCs (25)). Another illustration of the relevance of fine-tuned control of Zeb2 levels are miRs targeting Zeb2, and lncRNAs that regulate these miRs (68-71), with Zeb2 on its turn also controlling some of its own miR-encoding genes or clusters (72-74). In our ChIP-seq we find 125 peaks (~5% of the total) that correspond to the TSSs of 98 miR-genes (File S1). Among these miR-genes, Zeb2 binds to loci encoding miR-144, miR-148a, miR-9 and miR-153, known to target Zeb2 in the context of e.g., tumor progression (75-78). We recently added the identification, in human iPSCs subjected to ND, of *ZEB2* distant (~600 kb upstream) enhancers, which act through DNA-looping to the *ZEB2* promoter-proximal region (79). In addition, we have documented dynamic expression patterns of *Zeb2* in early embryos (27, 33, 80-82). We have also shown that cDNA-based expression of various tag-Zeb2 proteins is compatible with functional embryology-type and action mechanism studies (25, 38, 39). Importantly, our Zeb2-V5 allele enables normal production of tag-Zeb2 for the first time from its endogenous locus.

Only two studies present ZEB2 ChIP-seq data in human cells, i.e. SNU398 hepatocellular carcinoma and K562 erythroleukemia cells, respectively (31, 32). In K562 cells ZEB2 binds to the promoters of *NR4A2*, *NEUROG2* and *PITX3*, expressed in midbrain dopaminergic neurons, wherein Zeb2 negatively regulates axon growth and target innervation in mice (83). In SNU398, ZEB2 represses *GALNT3*, which is normally expressed in epithelial cells. This repression coincides with acquisition of a mesenchymal phenotype, linking ZEB2 here again to an EMT-like process. These two valuable studies also present limitations. The use of cancer cell lines of genomic instable nature may create possible bias in ChIP-seq, and in any case they overproduce ZEB2. Our ChIP-seq identifies >2,400 peaks for Zeb2-V5 in mESCs at ND-D8. This is in cells not stimulated with TGFβ family ligands, with 37.5% of Zeb2 sites mapping close to te TSSs (when defined as -10/+10kb). Most of these genes function in growth factor or cytokine signaling and/or encode transcriptional regulators, the latter suggesting that Zeb2 orchestrates other co-operating TFs driving the transcriptomic signature of NPCs. The regulation of Wnt signaling by Zeb2 is in line with observations that inhibition of the Wnt-βcatenin pathway suppresses ND *in vitro* and *in vivo*, and that Wnt (and Zeb2)-controlled *Tcf4* expression promotes neurogenesis and is required for normal brain development (84-88).

The 2,294 Zeb2 peaks map to 1,952 protein-coding genes, of which 1,244 are DEGs in ND-mESCs. Strikingly, the strongest enrichment of Zeb2 occurs on the *Zeb2* promoter itself, leading to the identification of a novel self-regulatory mechanism where Zeb2 binds upstream its TSS to maintain its

levels sufficiently high, also and at least during ND. While this autoregulation needs further investigation in Zeb2-dependent differentiation and/or maturation of other cell types (e.g. in cKO mouse models or in ND-iPSCs derived from appropriate MOWS patient cells), we propose that lower Zeb2 levels might compromise this autoregulatory loop. Deletion of the autoregulatory site from both *Zeb2* alleles (in the *ΔP/ΔP* cells), results in a significant decrease of Zeb2 mRNA levels but *Zeb2* is still partially expressed, and these cells can still exit from pluripotency and differentiate (contained in part within Fig. 5; *data not shown*). A number of genes, which are mainly linked to neuron maturation, are significantly affected in *Zeb2*$^{\Delta P/\Delta P}$ ESCs, whereas TGFβ/BMP-system component genes are not deregulated. Zeb2 dosage might thus underlie this difference in regulating its direct, ChIP+ genes in our ESCs. Zeb2 might be key to maintaining expression of neuronal genes, while for TGFβ/BMP-system genes Zeb2 may co-operate with other TFs (including p-Smads) or DNA-modifying enzymes to regulate the expression of target genes.

Zeb2 binds to receptor-activated phospho-Smads (pSmads), and several studies indicate its negative regulation of BMP-Smad activation of specific target genes, although Zeb2 also has Smad-independent functions (23, 29). BMP-pSmads bind to GGCGCC with high affinity (89). Morikawa and co-workers (90) have confirmed these results using ChIP-seq, and identified also a lower-affinity (so, higher BMP-doses required) BMP-Smad element (GGAGCC). For achieving full responsiveness it was proposed that the GG($^{A}/_{C}$)GCC element needs to be coupled with a Smad4 site, ideally located 5 bp away (90). We find that in primary targets affected by varying levels of Zeb2, E-boxes are located close to Smad-binding motifs. However, whether Zeb2 and Smads are co-present in target regions requires further experiments, such as ChiP-on-ChIP assays, and (non-neural) differentiation protocols (involving stimulation of the cells by addition of BMP and/or Nodal). However, these studies may be further complicated because of post-translational modification status of Zeb2, nuclear p-Smads and/or Smad4 (91-94).

Striking are also the 1,093 Zeb2-binding DEGs at D8. When we performed a gene-to-disease association using the human orthologues of these D8-DEGs, we found a clear association with several disorders (Fig. S6). These include neurodevelopmental, mental and ocular defects, which occur in MOWS. Altogether, our data may provide novel insights in MOWS due to suboptimal ZEB2 amounts in patients, and from now in includes an autoregulation aspect, as well as *ZEB2* as a putative modifier gene for many other congenital disorders.

Several *Zeb2*-cKO mouse models have been generated, and for many bulk RNA-seq data are available, from which here we selected two such data sets (23, 36, 95). In addition, similar data were obtained for cultured mESCs, either *Zeb2*-KO cells (25) or cells submitted to ND wherein e.g., Zeb2-KD was performed (37). Unfortunately, we could not include *Zeb2*-KO mESCs in these comparisons, for they convert less efficiently to EpiLSCs and fail to differentiate beyond this EpiLC state (25). The meta-analysis of these three different data sets, overlaid with the 1,952 Zeb2-V5 ChIP+ loci/genes, show therefore a limited number of common targets, *Cxcr4* being the only one common in all data

sets. This specifically narrows the Zeb2-bound gene collection to 108 in total. However, and interestingly, the latter enrich for GO terms such as pluripotency of stem cells, signaling by TGFβ and Wnt, cell fate commitment and neuron differentiation, all processes where Zeb2 plays a crucial role.

Out of these 108 genes, we selected 14 covering TGFβ/BMP signaling, pluripotency, neuron migration an differentiation/maturation, and checked their levels 2 days after Zeb2-KD at ND-D8. Most of these 14 genes relevant to NPC status showed to be critically depending on intact levels of Zeb2. They may help to explain why the defects caused by MOWS are observed later after birth and why (the few) missense mutations in MOWS (besides the more abundant significant deletions) present with milder syndromic manifestation. Both the cross-reference of Zeb2-ChIP+ genes with the transcriptome of ND-ESCs, and the meta-analysis, identify a number of common genes, such as *Bmp7*, *Tgfbr2*, *Tcf4*, *Smad1/2/3*, and *Sema3f* (File S3; Fig. S4), making Zeb2 a likely direct regulator of these genes. It is also intriguing that Zeb2 is recruited to and controlling *Tcf4* at D8, and that *Tcf4* is deregulated upon Zeb2-KD (using esiRNA (37) and shRNA here). Mutations in *TCF4* cause PTHS, a rare neurodevelopmental disorder with some defects overlapping with MOWS. The binding of Zeb2 to *Tcf4* opens new attractive roads to further investigate the crosstalk between these two TFs and their role in regulating crucial aspects of neurodevelopment.

Materials and Methods

ESC culture and differentiation

CGR8 (strain 129) wild-type and Zeb2-Flag-V5+ mESCs were cultured and differentiated towards the neural lineage (96, with few modifications). Briefly, mESCs were cultured on 0.1% Gelatin-coated plates in ESC-medium: DMEM supplemented with 15% heat-inactivated (HI) FBS, 2mM L-Glutamine, 1x Non-Essential Amino Acids (NEAA), 143 µM β-Mercapto-Ethanol (β-EtSH) (all ThermoFisher Scientific, TFS) and LIF (10^3 U/ml).

For ND, $4x10^6$ cells were plated on non-adherent 10-cm dishes (Greiner) and allowed to form cellular aggregates (CAs) in 10 ml CA-medium (DMEM, 10% HI-FBS, 2 mM L-Glutamine, 1x NEAA, and 143 µM β-EtSH). From D4 of ND, cells were grown in CA-medium supplemented with 5 µM Retinoic Acid (RA). During the aggregation stages of ND, medium was changed every other day by carefully collecting the aggregates with a 10-ml pipet and transferring them to a 15-ml conical tube. The CAs were allowed to sink to the bottom of the tube where, after the previous medium was carefully discarded, the CAs were then resuspended in fresh medium and transferred back to the dishes. At D8 of ND, the aggregates were harvested and dissociated by resuspension in 1 ml Accutase (TFS) and pipetting them up-and-down using a 1-ml pipet, after shaking them in a 37 □C water bath for 5 min. The Accutase was deactivated by adding 9 ml of fresh N2-medium (DMEM with 2 mM L-Glutamine, 50 µg BSA/ml and 1x N2-supplement) to the dissociated cells and pelleting the cells

gently for 5 min at 200 g. The cells were resuspended in fresh N2. To ensure single-cell suspension, the cells were filtered by passing them through a 40-mm nylon cell strainer (Corning). 2.5 x 10^5 cells/cm^2 were plated on Poly-DL-Ornithine hydrobromide (Sigma) / Laminin (Sigma) coated plates. Cells were harvested at D8 or D10 of ND.

Western blots

To check Zeb2-V5 protein, the 2BE3-clone ESCs were subjected to ND till D8. Cytoplasmic and nuclear fractions were extracted using NePer-kit® (TFS). Protein concentrations were measured using the Bradfort BCA (TFS) and equal quantities of protein lysates were loaded on 6% SDS-PAGs and thereafter cut based on protein relative molecular mass. Gels were then transferred onto nitrocellulose membranes (Amersham Bioscience), which were incubated overnight with anti-Zeb2 (20) and anti-V5 (Life Technologies) antibody, followed by incubation at RT with HorseRadish Peroxidase (HRP) conjugated secondary anti-rabbit and anti-mouse antibodies, respectively (Jackson ImmunoResearch). Protein bands corresponding to Zeb2 or Zeb2-V5 were visualized on an AI-600 digital imager (Amersham|). As loading control, we used Valosin-containing Protein (VCP) and anti-VCP antibody (Santa Cruz sc-57492, mouse).

RNA extraction and RT-qPCR analysis

Total RNA was extracted from ESCs using TRI Reagent (Sigma), and used for cDNA synthesis with RevertAid RT Kit (TFS) with oligodT-primers. RT-qPCR was performed using SybrGreen dye (BioRad) on a CFX96 T1000 thermal cycler (BioRad). All data shown are averages of 3 independent biological replicates and 3 technical replicates, normalized to β-Actin mRNA levels. Primers are listed in Table 2. Analysis and data visualization was performed in R environment for statistical computing version 3.5.3, implemented with the *tidyverse* version 1.3 package (https://github.com/tidyverse).

Tag-Zeb2 mouse ESCs

gRNAs (Table 1) targeting *Zeb2*-ex9, and tracrRNA (Integrated DNA Technologies, IDT), were diluted to 125 ng/µl in duplex buffer (IDT). gRNAs were annealed to tracrRNA at 1:1 ratio at 95°C for 5 min and cooling the samples to room temperature (RT, 24°C). 250 ng of these annealed gRNAs were transfected in 350,000 mESCs together with 2 µg pX459-Cas9-puro vector and 1 µg ssDNA oligo of the Donor Template containing the FlagV5-tag sequence (Table 1). Transfection was done in a gelatin-coated 6-well plate using DNA:Lipofectamine2000 (ratio of 1:2). Six hours after transfection the medium was refreshed, at 24 hours the cells were Puromycin-selected (2 µg/ml). After 2 days, the remaining cells were transferred to gelatin-coated 10-cm dishes and given fresh ESC-medium (see below). Per dish 1,000; 1,500; or 2,000 cells were plated and allowed to form colonies. Medium was

changed every other day. Colonies were picked, expanded and genotyped by PCR (both outer and inner primer sets were used (Table S1; Fig. S1). All candidate clones were validated by Sanger-sequencing; correct clones were expanded and validated by Western blot.

CRISPR/Cas9-mediated deletion of Zeb2 binding site located at chr2:45109746-45110421

Oligonucleotides for gRNAs (Table 1) with target outside of this chr2-region were cloned into *Bbs*I-digested pX330-hspCas9-T2A-eGFP plasmid. All plasmids were sequenced. 4 µg of gRNA-plasmids (1 µg each) were transfected in 350,000 mESCs and selected. After 24 hours these cells were sorted as GFP+ cells (Becton-Dickinson LSR Fortessa). Per well of a 6-well plate 1,000; 1,500; or 2,000 GFP+ cells were plated and colonies allowed to form, picked and genotyped by PCR using primers flanking this deletion, and within and outside of it. Clones showing a possible heterozygous or homozygous deletion, as concluded from the PCR analysis, were subjected to ND. At D8, they were harvested, RNA was isolated and cDNA synthesized (see below), and amplified (for the primers, see Table S1). All candidate clones were validated by Sanger-sequencing.

ChIP-seq

DNA libraries from input (i.e. control) and V5 ChIPs were prepared using ThruPLEX DNA protocol (TakaraBio) specific for low amounts of DNA, and sequenced on Illumina HiSeq-2500, and single reads of 50 bp were generated. Adapter sequences were trimmed from the 3'-end of the reads, after which the reads were aligned to the mm10/GRCm38 genome using HISAT2 (97). From the alignments, secondary, supplementary, low quality and fragmented alignments (fragments > 150 bp) were filtered away. Peaks were called with MACS (98), and coverage was determined. 42 and 25 million reads were generated for input and V5 ChIP, respectively.

ChIP-seq data analysis

Peak calling was performed with MACS2 (Galaxy version 2.1.1.20160309.6) (98, 99), with default parameters (narrow peak calling, *Mm*1.87e9, FDR < 0.05) using the input sample as background. The No model parameter was used, and the extension size was set on 210 bp based on the predicted fragment lengths from the alignments (MACS2 predict-tool, Galaxy version 2.1.1.20160309.1; 98, 99). The distance of the aligned reads from the TSS of the gene was analyzed using ComputeMatrix (Galaxy version 3.3.2.0.0) and PlotHeatmap Galaxy version 3.3.2.0.1; the used matrix is based on the log2ratio of the aligned ChIP peaks over the input, calculated using BamCompare (Galaxy version 3.3.2.0.0) (100).

Transcription Factors motifs enrichment analysis

To identify the TFBS in ZEB2 binding regions associated with DEGs, we first extracted unique ZEB2 peaks located 10kb +/- from TSS. Next, we analyzed the TFBS enrichment using UniBind enrichment tool with motifs from the UniBind database (using reference genome GRCm38/mm10) (101). As a background for the analysis all ZEB2 peaks were used. The p-value from Fisher's exact test after multitest adjustments was used to identify significantly enriched TFBS. Further, the max rank index calculated based on the odds ratio, p-value from Fisher's exact test and the number of overlapping regions, was applied to rank the top enriched motifs.

RNA-seq

The quality of total RNA (of biologically independent triplicates) of wild-type mESCs at D0, and at ND-D4, D6 and D8, was checked on Agilent Technologies-2100 Bioanalyzer, using an RNA nano-assay. All samples had RIN value of 9.8 or higher. Triplicate RNA-seq libraries were prepared (Illumina TruSeq stranded mRNA protocol; www.illumina.com). Briefly, 200 ng of total RNA was purified using polyT-oligo-attached magnetic beads for ending with polyA-RNA. The polyA-tailed RNA was fragmented, and cDNA synthesized (SuperScript II, random primers, in the presence of Actinomycin D). cDNA fragments were end-repaired, purified (AMPureXP beads), A-tailed using Klenow exo-enzyme and dATP. Paired-end adapters with dual index (Illumina) were ligated to the A-tailed cDNA fragments and purified (AMPureXP beads).

The resulting adapter-modified cDNAs were enriched by PCR (Phusion polymerase) as follows: 30 sec at 98°C, 15 cycles of (10 sec at 98°C, 30 sec at 60°C, 30 sec at 72°C), 5 min at 72°C. PCR products were purified (AMPureXP beads) and eluted in 30 µl resuspension buffer. One µl was loaded on an Agilent 2100 Bioanalyzer using a DNA-1000 assay to determine concentration and for quality check. Cluster generation was performed according to the Illumina TruSeq SR Rapid Cluster kit v2 Reagents Preparation Guide (www.illumina.com). After hybridization of the sequencing primer, sequencing-by-synthesis was performed using a HiSeq-2500 with a single-read 50-cycle protocol followed by dual index sequencing. Illumina adapter sequences have been trimmed off the reads, which were subsequently mapped against the GRCm38 mouse reference (using HiSat2 version 2.1.0; (97)). Gene expression values were called (using HTSeq-count version 0.9.1; 102) and Ensembl release 84 gene and transcript annotation. Sample QC and DEG analysis have been performed in the R environment for statistical computing (version 3.5.3, using DESeq2 version 1.22.1 and Tidyverse version 1.2.1 (https://github.com/tidyverse; https://www.r-project.org/; (103, R Core Team 2018 (104)).

Meta-analysis

RNA-seq datasets (as DEG tables) were downloaded from GEO (https://www.ncbi.nlm.nih.gov/geo/, GSE35616 and GSE103003, respectively). Cross-referencing and visualization was performed in R, using Tidyverse, VennDiagram and pheatmap packages.

Pathway-enrichment, GO, Function analysis and Gene-to-Disease association

Gene Onthology, pathway enrichment and function analysis were performed with StringDB package for R, while for Gene-to-Disease association Disgenet2R for R was used.

Data Availability Statement

Data are available upon kind request.

Acknowledgements

This work was supported mainly by Erasmus University Medical Center via departmental funds, extra funds coordinated with its Executive Board, and BIG project funding, a collaborative extra support between Erasmus University Rotterdam and its University Medical Center for promoting fundamental research at the Theme of Biomedical Sciences, and hence the Department of Cell Biology. We thank all co-workers of the Center for Biomics-Genomics at Erasmus University Medical Center for their expert technical assistance, and colleagues Frank Grosveld and Raymond Poot for constructive discussions.

Conflict of Interest Statement

The authors declare no conflict of interest.

References

1. Funahashi, J., Kamachi, Y., Goto, K. and Kondoh, H. (1991) Identification of nuclear factor delta EF1 and its binding site essential for lens-specific activity of the delta 1-crystallin enhancer. *Nucleic Acids Res.*, **19**, 3543-3547.
2. Sekido, R., Murai, K., Funahashi, J., Kamachi, Y., Fujisawa-Sehara, A., Nabeshima, Y. and Kondoh, H. (1994) The delta-crystallin enhancer-binding protein delta EF1 is a repressor of E2-box-mediated gene activation. *Mol. Cell. Biol.*, **14**, 5692-5700.
3. Remacle,, J.E., Kraft, H., Lerchner, W., Wuytens, G., Collart, C., Verschueren, K., Smith, J.C. and Huylebroeck, D. (1999) New mode of DNA binding of multi-zinc finger transcription factors: deltaEF1 family members bind with two hands to two target sites. *EMBO J.*, **18**, 5073-5084.
4. Verschueren, K., Remacle, J.E., Collart, C., Kraft, H., Baker, B.S., Tylzanowski, P., Nelles, L., Wuytens, G., Su, M.T., Bodmer, R., et al. (1999) SIP1, a novel zinc finger/homeodomain repressor, interacts with Smad proteins and binds to 5'-CACCT sequences in candidate target genes. *J. Biol. Chem.*, **274**, 20489-20498.
5. Mowat, D.R., Wilson, M.J. and Goossens, M. (2003) Mowat-Wilson syndrome. *J. Med. Genet.*, **40**, 305-310.
6. Cerruti Mainardi, P., Pastore, G., Zweier, C. and Rauch, A. (2004) Mowat-Wilson syndrome and mutation in the zinc finger homeo box 1B gene: a well-defined clinical entity. *J. Med. Genet.*, **41**, e16.
7. Ishihara, N., Yamada, K., Yamada, Y., Miura, K., Kato, J., Kuwabara, N., Hara, Y., Kobayashi, Y., Hoshino, K., Nomura, Y., et al. (2004) Clinical and molecular analysis of Mowat-Wilson syndrome associated with ZFHX1B mutations and deletions at 2q22-q24.1. *J. Med. Genet.*, **41**, 387-393.
8. Mowat, D.R., Croaker, G.D., Cass, D.T., Kerr, B.A., Chaitow, J., Adès, L.C., Chia, N.L. and Wilson, M.J. (1998) Hirschsprung disease, microcephaly, mental retardation, and characteristic facial features: delineation of a new syndrome and identification of a locus at chromosome 2q22-q23. *J. Med. Genet.* **35**, 617-623.
9. Cacheux, V., Dastot-Le Moal, F., Kääriäinen, H., Bondurand, N., Rintala, R., Boissier, B., Wilson, M., Mowat, D., and Goossens, M. (2001) Loss-of-function mutations in SIP1 Smad interacting protein 1 result in a syndromic Hirschsprung disease. *Hum. Mol. Genet.*, **10**, 1503-1510.
10. Wakamatsu, N., Yamada, Y., Yamada, K., Ono, T., Nomura, N., Taniguchi, H., Kitoh, H., Mutoh, N., Yamanaka, T., Mushiake, K., et al. (2001) Mutations in SIP1, encoding Smad interacting protein-1, cause a form of Hirschsprung disease. *Nat. Genet.*, **27**, 369-370.
11. Yamada, K., Yamada, Y., Nomura, N., Miura, K., Wakako, R., Hayakawa, C., Matsumoto, A., Kumagai, T., Yoshimura, I., Miyazaki, S., et al. (2001) Nonsense and frameshift mutations in ZFHX1B, encoding Smad-interacting protein 1, cause a complex developmental disorder with a great variety of clinical features. *Am. J. Hum. Genet.*, **69**, 1178-1185.
12. Wilson, M., Mowat, D., Dastot-Le Moal, F., Cacheux, V., Kääriäinen, H., Cass, D., Donnai, D., Clayton-Smith, J., Townshend, S., Curry, C., et al. (2003) Further delineation of the phenotype associated with heterozygous mutations in ZFHX1B. *Am. J. Med. Genet. A.*, **119A**, 257-265.
13. Zweier, C., Thiel, C.T., Dufke, A., Crow, Y.J., Meinecke, P., Suri, M., Ala-Mello, S., Beemer, F., Bernasconi, S., Bianchi, P., et al. (2005) Clinical and mutational spectrum of Mowat-Wilson syndrome. *Eur. J. Med. Genet.*, **48**, 97-111.
14. Zweier, C., Horn, D., Kraus, C. and Rauch A. (2006) Atypical ZFHX1B mutation associated with a mild Mowat-Wilson syndrome phenotype. *Am. J. Med. Genet A.*, **140A**, 869-872.
15. Garavelli, L., Zollino, M., Mainardi, P.C., Gurrieri, F., Rivieri, F., Soli, F., Verri, R., Albertini, E., Favaron, E., Zignani, M., et al. (2009) Mowat-Wilson syndrome: facial phenotype changing with age: study of 19 Italian patients and review of the literature. *Am. J. Med. Genet. A.*, **149A**, 417-426.
16. Ivanovski, I., Djuric, O., Caraffi, S.G., Santodirocco, D., Pollazzon, M., Rosato, S., Cordelli, D.M., Abdalla, E., Accorsi, P., Adam, M.P., et al. (2018) Phenotype and genotype of 87 patients with Mowat-Wilson syndrome and recommendations for care. *Genet. Med.*, **20**, 965-675.

17. Garavelli, L., Ivanovski, I., Caraffi, S.G., Santodirocco, D., Pollazzon, M., Cordelli, D.M., Abdalla, E., Accorsi, P., Adam, M.P., Baldo, C., et al. (2017) Neuroimaging findings in Mowat-Wilson syndrome: a study of 54 patients. *Genet. Med.*, **19**, 691-700.
18. Ricci, E., Fetta, A., Garavelli, L., Caraffi, S., Ivanovski, I., Bonanni, P., Accorsi, P., Giordano, L., Pantaleoni, C., Romeo, A., et al. (2021) Further delineation and long-term evolution of electroclinical phenotype in Mowat Wilson Syndrome. A longitudinal study in 40 individuals. *Epilepsy Behav.*, **124**, 108315.
19. Comijn, J., Berx, G., Vermassen, P., Verschueren, K., van Grunsven, L., Bruyneel, E., Mareel, M., Huylebroeck, D. and van Roy, F. (2001) The two-handed E box binding zinc finger protein SIP1 downregulates E-cadherin and induces invasion. *Mol. Cell.*, **7**, 1267-1278.
20. Seuntjens, E., Nityanandam, A., Miquelajauregui, A., Debruyn, J., Stryjewska, A., Goebbels, S., Nave, K.A., Huylebroeck, D. and Tarabykin, V. (2009) Sip1 regulates sequential fate decisions by feedback signalling from postmitotic neurons to progenitors. *Nat. Neurosci.*, **12**, 1373-1380.
21. Weng, Q., Chen, Y., Wang, H., Xu, X., Yang, B., He, Q., Shou, W., Chen, Y., Higashi, Y., van den Berghe, V., et al. (2012) Dual-mode modulation of Smad signalling by Smad-interacting protein Sip1 is required for myelination in the central nervous system. *Neuron*, **73**, 713-728.
22. Scott, C.L., Soen, B., Martens, L., Skrypek, N., Saelens, W., Taminau, J., Blancke, G., Van Isterdael, G., Huylebroeck, D., Haigh, J., et al. (2016) The transcription factor Zeb2 regulates development of conventional and plasmacytoid DCs by repressing Id2. *J. Exp. Med.*, **213**, 897-911.
23. Deryckere, A., Stappers, E., Dries, R., Peyre, E., van den Berghe, V., Conidi, A., Zampeta, F.I., Francis, A., Bresseleers, M., Stryjewska, A., et al. (2020) Multifaceted actions of Zeb2 in postnatal neurogenesis from the ventricular-subventricular zone to the olfactory bulb. *Development*, **147**, dev184861.
24. Wu, L.M., Wang, J., Conidi, A., Zhao, C., Wang, H., Ford, Z., Zhang, L., Zweier, C., Ayee, B.G., Maurel, P., et al. (2016) Zeb2 recruits HDAC-NuRD to inhibit Notch and controls Schwann cell differentiation and remyelination. *Nat. Neurosci.*, **19**, 1060-1072.
25. Stryjewska, A., Dries, R., Pieters, T., Verstappen, G., Conidi, A., Coddens, K., Francis, A., Umans, L., van IJcken, W.F., Berx, G., et al. (2017) Zeb2 Regulates Cell Fate at the Exit from Epiblast State in Mouse Embryonic Stem Cells. *Stem Cells*, **35**, 611-625.
26. Menuchin-Lasowski, Y., Dagan, B., Conidi, A., Cohen-Gulkar, M., David, A., Ehrlich, M., Giladi, P.O., Clark, B.S., Blackshaw, S., Shapira, K., et al. (2020) Zeb2 regulates the balance between retinal interneurons and Müller glia by inhibition of BMP-Smad signalling. *Dev. Biol.*, **468**, 80-92.
27. Lerchner, W., Latinkic, B.V., Remacle, J.E., Huylebroeck, D. and Smith, J.C. (2000). Region-specific activation of the Xenopus brachyury promoter involves active repression in ectoderm and endoderm: a study using transgenic frog embryos. *Development*, **127**, 2729-2739.
28. van Grunsven, L.A., Taelman, V., Michiels, C., Opdecamp, K., Huylebroeck, D. and Bellefroid, E.J. (2006) deltaEF1 and SIP1 are differentially expressed and have overlapping activities during Xenopus embryogenesis. *Dev. Dyn.*, **235**, 1491-1500.
29. Conidi, A., Cazzola, S., Beets, K., Coddens, K., Collart, C., Cornelis, F., Cox, L., Debruyn, J., Dobreva, M.P., Dries, R., et al. (2011) Few Smad proteins and many Smad-interacting proteins yield multiple functions and action modes in TGFβ/BMP signalling in vivo. *Cytokine Growth Factor Rev.*, **22**, 287-300.
30. Birkhoff, J., Huylebroeck, D. and Conidi, A. (2021) ZEB2, the Mowat-Wilson Syndrome transcription factor: confirmations, novel functions, and continuing surprises. *Genes*, **12**, 1037.
31. Balcik-Ercin, P., Cetin, M., Yalim-Camci, I., Odabas, G., Tokay, N., Sayan, A.E. and Yagci, T. (2018) Genome-wide analysis of endogenously expressed ZEB2 binding sites reveals inverse correlations between ZEB2 and GalNAc-transferase GALNT3 in human tumors. *Cell. Oncol. (Dordr).*, **41**, 379-393.
32. Yang, S., Toledo, E.M., Rosmaninho, P., Peng, C., Uhlén, P., Castro, D.S. and Arenas, E. (2018) A Zeb2-miR-200c loop controls midbrain dopaminergic neuron neurogenesis and migration. *Commun. Biol.*, **1**, 75.

33. Miyoshi, T., Maruhashi, M., Van de Putte, T., Kondoh, H., Huylebroeck, D. and Higashi, Y. (2006) Complementary expression pattern of Zfhx1 genes Sip1 and deltaEF1 in the mouse embryo and their genetic interaction revealed by compound mutants. *Dev. Dyn.*, **235**, 1941-1952.
34. Vandamme, N., Denecker, G., Bruneel, K., Blancke, G., Akay, Ö., Taminau, J., De Coninck, J., De Smedt, E., Skrypek, N., Van Loocke, W., et al. (2020) The EMT Transcription Factor ZEB2 Promotes Proliferation of Primary and Metastatic Melanoma While Suppressing an Invasive, Mesenchymal-Like Phenotype. *Cancer Res.*, **80**, 2983-2995.
35. Nelles, L., Van de Putte, T., van Grunsven, L., Huylebroeck, D. and Verschueren, K. (2003) Organization of the mouse Zfhx1b gene encoding the two-handed zinc finger repressor Smad-interacting protein-1. *Genomics*, **82**, 460-469.
36. van den Berghe, V., Stappers, E., Vandesande, B., Dimidschstein, J., Kroes, R., Francis, A., Conidi, A., Lesage, F., Dries, R., Cazzola, S., et al. (2013) Directed migration of cortical interneurons depends on the cell-autonomous action of Sip1. *Neuron*, **77**, 70-82.
37. Dries, R., Stryjewska, A., Coddens, K., Okawa, S., Notelaers, T., Birkhoff, J., Dekker, M., Verfaillie, C.M., Del Sol, A., Mulugeta, E., et al. (2020) Integrative and perturbation-based analysis of the transcriptional dynamics of TGFβ/BMP system components in transition from embryonic stem cells to neural progenitors. *Stem Cells*, **38**, 202-217.
38. Papin, C., van Grunsven, L.A., Verschueren, K., Huylebroeck, D. and Smith, J.C. (2002) Dynamic regulation of Brachyury expression in the amphibian embryo by XSIP1. *Mech. Dev.*, **111**, 37-46.
39. Verstappen, G., van Grunsven, L.A., Michiels, C., Van de Putte, T., Souopgui, J., Van Damme, J., Bellefroid, E., Vandekerckhove, J. and Huylebroeck, D. (2008) Atypical Mowat-Wilson patient confirms the importance of the novel association between ZFHX1B/SIP1 and NuRD corepressor complex. *Hum. Mol. Genet.*, **17**, 1175-1183.
40. Afgan, E., Baker, D., Batut, B., van den Beek, M., Bouvier, D., Cech, M., Chilton, J., Clements, D., Coraor, N., Gruning, B.A., et al. (2018) The Galaxy platform for accessible, reproducible and collaborative biomedical analyses: 2018 update. *Nucleic Acids Res.*, **46**, W537-W544.
41. Sepp, M., Pruunsild, P. and Timmusk, T. (2012) Pitt-Hopkins syndrome-associated mutations in TCF4 lead to variable impairment of the transcription factor function ranging from hypomorphic to dominant-negative effects. *Hum. Mol. Genet.*, **21**, 2873-2888.
42. Teixeira, J.R., Szeto, R.A., Carvalho, V.M.A., Muotri, A.R. and Papes, F. (2021) Transcription factor 4 and its association with psychiatric disorders. *Transl. Psychiatry*, **11**, 19.
43. Corneliussen, B., Thornell, A., Hallberg, B. and Grundstrom, T. (1991) Helix-loop-helix transcriptional activators bind to a sequence in glucocorticoid response elements of retrovirus enhancers. *J. Virol.*, **65**, 6084-6093.
44. Forrest, M.P., Hill, M.J., Quantock, A.J., Martin-Rendon, E. and Blake, D.J. (2014) The emerging roles of TCF4 in disease and development. *Trends Mol. Med.*, **20**, 322-31.
45. Wang, L.H., and Baker, N.E. (2015) E Proteins and ID Proteins: Helix-Loop-Helix Partners in Development and Disease. *Dev. Cell*, **35**, 269-280.
46. Fu, H., Cai, J., Clevers, H., Fast, E., Gray, S., Greenberg, R., Jain, M.K., Ma, Q., Qiu, M., Rowitch, D.H., et al. (2009) A genome-wide screen for spatially restricted expression patterns identifies transcription factors that regulate glial development. *J. Neurosci.*, **29**, 11399-11408.
47. Brockschmidt, A., Todt, U., Ryu, S., Hoischen, A., Landwehr, C., Birnbaum, S., Frenck, W., Radlwimmer, B., Lichter, P., Engels, H. et al. (2007) Severe mental retardation with breathing abnormalities (Pitt-Hopkins syndrome) is caused by haploinsufficiency of the neuronal bHLH transcription factor TCF4. *Hum. Mol. Genet.*, **16**, 1488-1494.
48. Zhang T, Zhang Z, Dong Q, Xiong J, Zhu B. Histone H3K27 acetylation is dispensable for enhancer activity in mouse embryonic stem cells. Genome Biol. 2020 Feb 21;21(1):45. doi: 10.1186/s13059-020-01957-w. PMID: 32085783; PMCID: PMC7035716.
49. Suh H, Consiglio A, Ray J, Sawai T, D'Amour KA, Gage FH. In vivo fate analysis reveals the multipotent and self-renewal capacities of Sox2+ neural stem cells in the adult hippocampus. Cell Stem Cell. 2007 Nov;1(5):515-28.

50. Quintes S, Brinkmann BG, Ebert M, Fröb F, Kungl T, Arlt FA, Tarabykin V, Huylebroeck D, Meijer D, Suter U, Wegner M, Sereda MW, Nave KA. Zeb2 is essential for Schwann cell differentiation, myelination and nerve repair. Nat Neurosci. 2016 Aug;19(8):1050-9.
51. Dunn SJ, Martello G, Yordanov B, Emmott S, Smith AG. Defining an essential transcription factor program for naïve pluripotency. Science. 2014 344(6188):1156-60.
52. Rao C, Malaguti M, Mason JO, Lowell S. The transcription factor E2A drives neural differentiation in pluripotent cells. Development. 2020 Jun 22;147(12):dev184093. doi: 10.1242/dev.184093. PMID: 32487737; PMCID: PMC7328008.
53. El Wakil A, Francius C, Wolff A, Pleau-Varet J, Nardelli J. The GATA2 transcription factor negatively regulates the proliferation of neuronal progenitors. Development. 2006 Jun;133(11):2155-65
54. Beagan JA, Duong MT, Titus KR, et al. YY1 and CTCF orchestrate a 3D chromatin looping switch during early neural lineage commitment. Genome Res. 2017;27(7):1139–52.
55. Hegarty, S.V., Sullivan, A.M. and O'Keeffe, G.W. (2015) Zeb2: A multifunctional regulator of nervous system development. *Prog. Neurobiol.*, **132**, 81-95.
56. Stumm, R.K., Zhou, C., Ara, T., Lazarini, F., Dubois-Dalcq, M., Nagasawa, T., Hollt, V. and Schulz, S. (2003) CXCR4 regulates interneuron migration in the developing neocortex. *J. Neurosci.*, **23**, 5123-5130.
57. Nash, B. and Meucci, O. (2014) Functions of the chemokine receptor CXCR4 in the central nervous system and its regulation by mu-opioid receptors. *Int. Rev. Neurobiol.*, **118**, 105-128.
58. Georgala, P.A., Carr, C.B. and Price, D.J. (2011) The role of Pax6 in forebrain development. *Dev. Neurobiol.*, **71**, 690-709.
59. Dias, C.M., Punetha, J., Zheng, C., Mazaheri, N., Rad, A., Efthymiou, S., Petersen, A., Dehghani, M., Pehlivan, D., Partlow, J.N., et al. (2019) Homozygous Missense Variants in NTNG2, Encoding a Presynaptic Netrin-G2 Adhesion Protein, Lead to a Distinct Neurodevelopmental Disorder. *Am. J. Hum. Genet.*, **105**, 1048-1056.
60. Lui, N.C., Tam, W.Y., Gao, C., Huang, J.D., Wang, C.C., Jiang, L., Yung, W.H. and Kwan, K.M. (2017) Lhx1/5 control dendritogenesis and spine morphogenesis of Purkinje cells via regulation of Espin. *Nat. Commun.*, **8**, 15079.
61. Tzeng, S.F. and de Vellis, J. (1998) Id1, Id2, and Id3 gene expression in neural cells during development. *Glia*, **24**, 372-381.
62. Blomfield, I.M., Rocamonde, B., Masdeu, M.D.M., Mulugeta, E., Vaga, S., van den Berg, D.L., Huillard, E., Guillemot, F. and Urban, N. (2019) Id4 promotes the elimination of the pro-activation factor Ascl1 to maintain quiescence of adult hippocampal stem cells. *Elife*, **8**, e48561.
63. Havrda, M.C., Harris, B.T., Mantani, A., Ward, N.M., Paolella, B.R., Cuzon, V.C., Yeh, H.H. and Israel, M.A. (2008) Id2 is required for specification of dopaminergic neurons during adult olfactory neurogenesis. *J. Neurosci.*, **28**, 14074-14086.
64. Remacle, J.E., Kraft, H., Lerchner, W., Wuytens, G., Collart, C., Verschueren, K., Smith, J.C. and Huylebroeck, D. (1999) New mode of DNA binding of multi-zinc finger transcription factors: deltaEF1 family members bind with two hands to two target sites. *EMBO J.*, **18**, 5073-5084.
65. Hill, C.S. (2016) Transcriptional Control by the SMADs. *Cold Spring Harb. Perspect. Biol.*, **8**, a022079.
66. Higashi, Y., Maruhashi, M., Nelles, L., Van de Putte, T., Verschueren, K., Miyoshi, T., Yoshimoto, A., Kondoh, H. and Huylebroeck, D. (2002) Generation of the floxed allele of the SIP1 (Smad-interacting protein 1) gene for Cre-mediated conditional knockout in the mouse. *Genesis*, **32**, 82-84.
67. van Helden, M.J., Goossens, S., Daussy, C., Mathieu, A.L., Faure, F., Marcais, A., Vandamme, N., Farla, N., Mayol, K., Viel, S., et al. (2015) Terminal NK cell maturation is controlled by concerted actions of T-bet and Zeb2 and is essential for melanoma rejection. *J. Exp. Med.*, **212**, 2015-2025.
68. Guan, J., Liu, P., Wang, A. and Wang, B. (2020) Long noncoding RNA ZEB2AS1 affects cell proliferation and apoptosis via the miR1225p/PLK1 axis in acute myeloid leukemia. *Int. J. Mol. Med.*, **46**, 1490-1500.

69. Jiang, Y., Wu, K., Cao, W., Xu, Q., Wang, X., Qin, X., Wang, X., Li, Y., Zhang, J. and Chen, W. (2020) Long noncoding RNA KTN1-AS1 promotes head and neck squamous cell carcinoma cell epithelial-mesenchymal transition by targeting miR-153-3p. *Epigenomics*, **12**, 487-505.
70. Yao, H., Hou, G., Wang, Q.Y., Xu, W.B., Zhao, H.Q. and Xu, Y.C. (2020) LncRNA SPRY4IT1 promotes progression of osteosarcoma by regulating ZEB1 and ZEB2 expression through sponging of miR101 activity. *Int. J. Oncol.*, **56**, 85-100.
71. Cheng, H., Zhao, H., Xiao, X., Huang, Q., Zeng, W., Tian, B., Ma, T., Lu, D., Jin, Y. and Li, Y.(2021) Long Non-coding RNA MALAT1 Upregulates ZEB2 Expression to Promote Malignant Progression of Glioma by Attenuating miR-124. *Mol. Neurobiol.*, **58**, 1006-1016.
72. Brabletz, S. and Brabletz, T. (2010) The ZEB/miR-200 feedback loop--a motor of cellular plasticity in development and cancer? *EMBO Rep.*, **11**, 670-677.
73. Exposito-Villen, Aránega, E.A. and Franco, D. (2018) Functional Role of Non-Coding RNAs during Epithelial-To-Mesenchymal Transition. *Noncoding RNA*, **4**, 14.
74. Gregory, P.A., Bracken, C.P., Bert, A.G. and Goodall, G.J. (2008) MicroRNAs as regulators of epithelial-mesenchymal transition. *Cell Cycle*, **7**, 3112-3118.
75. Guan, H., Liang, W., Xie, Z., Li, H., Liu, J., Liu, L., Xiu, L. and Li, Y. (2015) Down-regulation of miR-144 promotes thyroid cancer cell invasion by targeting ZEB1 and ZEB2. *Endocrine*, **48**, 566-574.
76. Pan, Y., Zhang, J., Fu, H. and Shen, L. (2016) miR-144 functions as a tumor suppressor in breast cancer through inhibiting ZEB1/2-mediated epithelial mesenchymal transition process. *Onco Targets Ther.*, **9**, 6247-6255.
77. Nourmohammadi, B., Tafsiri, E., Rahimi, A., Nourmohammadi, Z., Daneshvar Kakhaki, A., Cho, W. and Karimipoor, M. (2019) Expression of miR-9 and miR-200c, ZEB1, ZEB2 and E-cadherin in Non-Small Cell Lung Cancers in Iran. *Asian Pac. J. Cancer Prev.*, **20**, 1633-1639.
78. Wahab, N.A., Othman, Z., Nasri, N.W.M., Mokhtar, M.H., Ibrahim, S.F., Hamid, A.A., Raja Ali, R.A. and Mokhtar, N.M. (2020) Inhibition of miR-141 and miR-200a Increase DLC-1 and ZEB2 Expression, Enhance Migration and Invasion in Metastatic Serous Ovarian Cancer. *Int. J. Environ. Res. Public Health*, **17**, 2766.
79. Birkhoff, J.C., Brouwer, R.W.W., Kolovos, P., Korporaal, A.L., Bermejo-Santos, A., Boltsis, I., Nowosad, K., van den Hout, M., Grosveld, F.G., van IJcken, W.F.J., et al. (2020) Targeted chromatin conformation analysis identifies novel distal neural enhancers of ZEB2 in pluripotent stem cell differentiation. *Hum. Mol. Genet.*, **29**, 2535-2550.
80. van Grunsven, L.A., Papin, C., Avalosse, B., Opdecamp, K., Huylebroeck, D., Smith, J.C. and Bellefroid, E.J. (2000) XSIP1, a Xenopus zinc finger/homeodomain encoding gene highly expressed during early neural development. *Mech. Dev.*, **94**, 189-193.
81. Van de Putte, T., Maruhashi, M., Francis, A., Nelles, L., Kondoh, H., Huylebroeck, D. and Higashi, Y. 92003) Mice lacking ZFHX1B, the gene that codes for Smad-interacting protein-1, reveal a role for multiple neural crest cell defects in the etiology of Hirschsprung disease-mental retardation syndrome. *Am. J. Hum. Genet.*, **72**, 465-470.
82. Takagi, T., Nishizaki, Y., Matsui, F., Wakamatsu, N. and Higashi, Y. (2015) De novo inbred heterozygous Zeb2/Sip1 mutant mice uniquely generated by germ-line conditional knockout exhibit craniofacial, callosal and behavioral defects associated with Mowat-Wilson syndrome. *Hum. Mol. Genet.*, **24**, 6390-6402.
83. Hegarty, S.V., Wyatt, S.L., Howard, L., Stappers, E., Huylebroeck, D., Sullivan, A.M. and O'Keeffe, G.W. (2017) Zeb2 is a negative regulator of midbrain dopaminergic axon growth and target innervation. *Sci. Rep.*, **7**, 8568.
84. Hirabayashi, Y., Itoh, Y., Tabata, H., Nakajima, K., Akiyama, T., Masuyama, N. and Gotoh, Y. (2004) The Wnt/beta-catenin pathway directs neuronal differentiation of cortical neural precursor cells. *Development*, **131**, 2791-2801.
85. Slawny, N.A, and O'Shea, K.S. (2011) Dynamic changes in Wnt signalling are required for neuronal differentiation of mouse embryonic stem cells. *Mol. Cell. Neurosci.*, **48**, 205-216.
86. Li, M., Santpere, G., Imamura Kawasawa, Y., Evgrafov, O.V., Gulden, F.O., Pochareddy, S., Sunkin, S.M., Li, Z., Shin, Y., Zhu, Y., et al. (2018) Integrative functional genomic analysis of human brain development and neuropsychiatric risks. *Science*, **362**, eaat7615.

87. Li, H., Zhu, Y., Morozov, Y.M., Chen, X., Page, S.C., Rannals, M.D., Maher, B.J. and Rakic, P. 92019) Disruption of TCF4 regulatory networks leads to abnormal cortical development and mental disabilities. *Mol. Psychiatry*, **24**, 1235-1246.
88. Mesman, S., Bakker, R. and Smidt, M.P. (2020) Tcf4 is required for correct brain development during embryogenesis. *Mol. Cell. Neurosci.*, **106**, 103502.
89. BabuRajendran, N., Palasingam, P., Narasimhan, K., Sun, W., Prabhakar, S., Jauch, R. and Kolatkar, P.R. (2010) Structure of Smad1 MH1/DNA complex reveals distinctive rearrangements of BMP and TGF-beta effectors. *Nucleic Acids Res.*, **38**, 3477-3488.
90. Morikawa, M., Koinuma, D., Tsutsumi, S., Vasilaki, E., Kanki, Y., Heldin, C.-H, Aburatani, H. and Miyazono, K. (2011) ChIP-seq reveals cell type-specific binding patterns of BMP-specific Smads and a novel binding motif. *Nucleic Acids Res.*, **39**, 8712-8727.
91. Liu, S., Long, J., Yuan, B., Zheng, M., Xiao, M., Xu, J., Lin, X. and Feng, X.H. (2016) SUMO Modification Reverses Inhibitory Effects of Smad Nuclear Interacting Protein-1 in TGF-beta Responses. *J. Biol. Chem.*, **291**, 24418-24430.
92. Xu, P., Lin, X. and Feng, X.H. (2016) Posttranslational Regulation of Smads. *Cold Spring Harb. Perspect. Biol.*, **8**, a022087.
93. Kim, Y.J., Kang, M.J., Kim, E., Kweon, T.H., Park, Y.S., Ji, S., Yang, W.H., Yi, E.C., and Cho, J.W. (2020) O-GlcNAc stabilizes SMAD4 by inhibiting GSK-3beta-mediated proteasomal degradation. *Sci. Rep.*, **10**, 19908.
94. Lin, X., Wang, Y., Jiang, Y., Xu, M., Pang, Q., Sun, J., Yu, Y., Shen, Z., Lei, R. and Xu, J. (2020) Sumoylation enhances the activity of the TGF-beta/SMAD and HIF-1 signalling pathways in keloids. *Life Sci.*, **255**, 117859.
95. McKinsey, G.L., Lindtner, S., Trzcinski, B., Visel, A., Pennacchio, L.A., Huylebroeck, D., Higashi, Y. and Rubenstein, J.L. (2013) Dlx1&2-dependent expression of Zfhx1b (Sip1, Zeb2) regulates the fate switch between cortical and striatal interneurons. *Neuron*, **77**, 83-98.
96. Bibel M, Richter J, Lacroix E, Barde YA. (2007) Generation of a defined and uniform population of CNS progenitors and neurons from mouse embryonic stem cells. *Nat Protoc*. **2(5):**1034-43.
97. Kim, D., Langmead, B. and Salzberg, S.L. (2015) HISAT: a fast spliced aligner with low memory requirements. *Nat. Methods*, **12**, 357-360.
98. Zhang, Y., Liu, T., Meyer, C.A., Eeckhoute, J., Johnson, D.S., Bernstein, B.E., Nusbaum, C., Myers, R,M., Brown, M., Li, W. et al. (2008) Model-based analysis of ChIP-Seq (MACS). *Genome Biol.*, **9**, R137.
99. Feng, J., Liu, T., Qin, B., Zhang, Y. and Liu, X.S. (2012) Identifying ChIP-seq enrichment using MACS. *Nat. Protoc.*, **7**, 1728-1740.
100. Ramirez, F., Ryan, D.P., Gruning, B., Bhardwaj, V., Kilpert, F., Richter, A.S., Heyne, S., Dundar, F. and Manke, T. (2016) deepTools2: a next generation web server for deep-sequencing data analysis. *Nucleic Acids Res.*, **44**, W160-165.
101. Puig RR, Boddie P, Khan A, Castro-Mondragon JA, Mathelier A. UniBind: maps of high-confidence direct TF-DNA interactions across nine species. BMC Genomics. 2021 Jun 26;22(1):482. doi: 10.1186/s12864-021-07760-6. PMID: 34174819; PMCID: PMC8236138.
102. Anders, S., Pyl, P.T. and Huber, W. (2015) HTSeq--a Python framework to work with high-throughput sequencing data. *Bioinformatics*, **31**, 166-169.
103. Love, M.I. and Huber, W. (2014) Anders S. Moderated estimation of fold change and dispersion for RNA-seq data with DESeq2. *Genome Biol.*, **15**, 550.
104. R Core Team, 2018. R: A language and environment for statistical computing. R Foundation for Statistical Computing, Vienna, Austria. https://www.r-project.org/

Legends to Figures

Figure 1. Characterization of the heterozygous Zeb2-Flag-V5 mESC line and ChIP-qPCR validation.

A) Allele-specific RT-qPCR using two sets of primers located either in exon7 (and therefore able to detect the whole Zeb2 mRNA produced by both alleles; orange bar) or located in exon9 and the V5-tag (thus recognizing specifically the knocked-in tagged allele; light blue bar). B) Western blot analysis showing V5 epitope containing Zeb2 in ES cell derived NPCs (at D8 of neural differentiation, ND) in nuclear extracts (NE), but not in cytoplasmic extracts (CE). Membranes were blotted with anti-V5 antibody (left panel, αV5) or anti-Zeb2 antibody (right panel, αZeb2 (20). As control, a fraction of Zeb2-rich extract obtained from HeLa cells transfected with pcDNA3-V5Zeb2 vector was also separated in the same gel. C) Zeb2 mRNA levels in wild-type (WT, orange bar) and Zeb2-V5 (grey bar, clone 2BE3, indicated as Zeb2-V5) mESCs during ND. D) Pluripotency markers *Nanog*, *Pou5f1* (*Oct4*) and *Sox2* are down regulated in Zeb2-V5 mESCs similarly to WT. The neuronal marker *Pax6* is also significantly upregulated during differentiation, like in WT mESCs. E) Scheme of the mouse *Cdh1* promoter showing the three E-boxes located upstream the ATG start codon. Zeb2 binds specifically to only two of these, indicated as R1 (25). F) ChIP-qPCR showing enrichment for Zeb2-V5 binding to the R1 region of the *Cdh1* promoter. Agarose beads were used as negative control (in grey).

Figure 2. Zeb2V5 protein is mainly recruited at the TSS of transcriptional regulator encoding genes, predominantly those classified in Wnt signaling.

A) 2,432 peaks were selected from our ChIP-seq data set (see Materials and Methods). Of these, 94% are associated with protein coding loci, 5% with miRNAs and the remaining 1% map to regions without functional annotation (NA). B) Frequency plot showing the binding of Zeb2V5 at and around (-10 to +10 kb) the TSS. C) The 2,294 peaks map to 1,952 protein encoding genes, many of which operate in Wnt signaling (File S1) or are (shown in D) transcriptional regulators. E) Of the 1,952 protein encoding genes, 1,244 are differentially expressed during ND, when compared to the undifferentiated state (at D0). Of these 1,244 genes, 335 are differentially expressed at all three time points of ND. A few examples are listed of DEGs uniquely expressed at one time point, as well as these that are shared among three time points; a full list is provided in File S2. F) Overlap of the Zeb2 bound regions with H3K27ac, H3K4me1 and H3K4me3 histone marks in the -10/+10 kb from the TSS of up- or down-regulated genes at D8 of mESCs differentiation. G) Overlap of the Zeb2 bound regions outside the -10/+10kb region from the TSS with histone marks.

Figure 3. Schematic representation of the meta-analysis Zeb2-bound genes versus RNA-seq datasets.

A) 108 genes bound by Zeb2 are also differentially expressed in the three datasets from other studies in mouse models and ESCs. *Cxcr4* is the only DEG bound by Zeb2 and common among the three datasets. B) These 108 genes mainly map to signaling pathways regulating stem cell pluripotency, and effects of TGFβ family, FoxO, and Hippo signaling/activity.

Figure 4. shRNA-mediated KD of Zeb2 discriminate between primary and secondary target genes.

A) Schematic overview of the shRNA transfection targeting Zeb2 (shZeb2) and read-out of the effect. Cellular aggregates at D8 of ND are dissociated and transfected with shZeb2 or against a scrambled, control sequence (shCTRL). Read-out is done two days after the start of shRNA addition. The list of shRNAs is given in Table S2. B) *Zeb2* levels after KD were reduced to 40-50% of their normal level (shZeb2, orange bars) compared to shCTRL (blue bars). *Bmp7*, *Cited2*, *Nanog*, *Sema3f*, *Smad1*, *Smad2*, *Smad3*, and *Tgfbr2* were significantly upregulated following Zeb2 KD, whereas genes encoding for neuronal specification and migration (*Cxcr4*, *Lhx5*, *Ntng2*, *Pax6* and *Tcf4*) were downregulated.

Figure 5. Deletion of the Zeb2-binding, candidate autoregulatory site (chr2:45109746-45110421) impairs Zeb2 mRNA levels and neuronal markers.

A) Schematic overview of the log(FoldEnrichment) of the peaks identified by ChIP-seq located in the mouse *Zeb2* locus, and localization on top of *Zeb2* intron/exon structure. The highest peak is located 232 bp upstream of the first translated exon. Grey arrow indicates the TSS of *Zeb2*. B) Zeb2 mRNA levels are strongly reduced in the $Zeb2^{\Delta P/\Delta P}$ clone. Expression levels (mRNA) of the target genes validated with shRNA (Figure 4). Most, but not all of the genes found to be affected following Zeb2 KD are also deregulated in $Zeb2^{\Delta P/\Delta P}$ mESCs in particular *Id2* and the neuronal markers *Cxcr4*, *Lhx5*, *Ntng2*, *Pax6* and *Tcf4*.

Tables

Table 1: **gRNAs and donor template used for CRISPR/Cas9-mediated *Zeb2* editing.**

Name	**Sequence**	**CRISPR/Cas9**
FlagV5 Donor Template	aaaatggaaaccaaatcagaccacgaagaagacaatatggaa gatggcatcgaaGACTACAAAGACGATGACG ACAAG***gatatc***GGTAAGCCTATCCCTAAC CCTCTCCTCGGTCTCGATTCTACG**TAA**a ctactgcattttaagcttcctattttttttccagtagtattgtt	In-frame knock-in of Flag-V5 tag
gRNA_ex9_1	GGAAACCAAATCAGACCACGAGG	
gRNA_ΔZP1	CCCGCGCGCGTTTCAATGGGCGC	Zeb2 peak deletion
gRNA_ΔZP2	CCCTCGCGAGTGCAACACACCAA	
gRNA_ΔZP3	GGGCTCGGAGCGCTGCCGATCGG	
gRNA_ΔZP4	CCGCTGGACCGGGGGGGAGTTGA	

Donor template: lowercase: homology arms located in exon 9 and 3'-UTR of *Zeb2*, underlined lowercase: mutated PAM sequences, uppercase: *FLAG* coding sequence, lowercase italics bold: *Eco*RI restriction site, underlined uppercase: *V5* coding sequence, bold uppercase: STOP codon.

Legends to Supplemental Figures

Figure S1. Characterization of the Zeb2-V5 mESC clone.

A) Schematic overview of the design strategy, including showing also primers used for genotyping and detection of tagged allele. B) Genotyping results (selected part) showing the heterozygous band (red arrow) present in mouse (m) ESC clone 2BE3. Lower band represents the wild-type (WT) allele. C) Zeb2-V5 specific PCR showing the presence of the tagged allele only in clone 2BE3, and not in WT genomic DNA material. Clone 1BD4 was also used as negative control. D) Sanger DNA-sequencing results of clone 2BE3 showing the alignment with the Zeb2V5 sequence designed *in silico*. The last three amino acids (i.e. GME) of WT Zeb2 have been modified in DK to remove a PAM sequence and mutate the remaining PAM sequence, target of the gRNA, to avoid multiple cutting of the CAS9. An *Eco*RI restriction site was inserted between the Flag and the V5 coding sequences to facilitate for screening and an artificial STOP codon was added after the V5-coding sequence.

Figure S2. Cross-reference of Zeb2Flagv5-bound protein-coding genes and transcriptome of differentiating mESCs.

A) Volcano plots showing the distribution of Zeb2 bound genes in the whole transcriptomes of D4, D6 and D8 neural differentiated mESCs. Red dots depict the genes bound by Zeb2 and grey crosses those not bound. B) About 12% of the up- or down-regulated genes are bound by Zeb2 (red bars) at D8 and the percentage does not change when expanding our analysis to the other points of differentiation. C) Of the 1,952 genes bound by Zeb2 and found being differentially expressed during mESC differentiation, 335 are in common among the three considered time points. *Zeb2* itself is among these common genes and its expression increases during differentiation (yellow dot). The volcano plots show the distribution of the common genes during differentiation. D) Timepoint specific DEGs depicted as volcano plots. The grey arrow in D8 panel indicates *Tcf4*.

Figure S3: Top 10 TF motifs enrichment at peaks present in -10/+10 kb from the TSS of up- or down-regulated genes

Scatter plots represent the top 10 TF motifs found in the peaks present in the -10/+10 kb from the TSS range in genes which are up- or down-regulated during mESCs neural differentiation (panel A and B respectively). Each dot represent a peak.

Figure S4. Expression of genes resulting from the meta-analysis of Zeb2-bound genes vs three independent RNA-seq datasets.

Heatmap visualizes the log2FoldChange of the resulting genes during mESC differentiation. RNA-seq datasets where the genes have been found to be differentially expressed are annotated as green (Nkx2.1|Zeb2), purple (Zeb2 KD in mESCs) or yellow (Gsh2|Zeb2) squares.

Figure S5. Genotyping of *Zeb2*$^{\Delta P/\Delta P}$ mESCs.

A) Primers (listed in Table 1) used for genotyping. B) PCR confirming the proper deletion of the selected region in clone E9.C) Further PCR showing the difference in molecular weight for regions amplified with different set of primers and discriminating between WT, heterozygous (*Zeb2*$^{\Delta P/+}$) and homozygous (*Zeb2*$^{\Delta P/\Delta P}$**)** deletion clones.D) Sanger sequencing showing the correct deletion of the selected region in the *Zeb2*$^{\Delta P/\Delta P}$ clone.

Figure S6. Distribution of Zeb binding sites (performed as single E-boxes; for details, see text) **and TGFβ/BMP activated (phospho-)Smads and Smad4 binding elements within the identified Zeb2-bound regions for primary target genes.**

A) Grey triangles represent distance from the TSS, while blue triangles depict the TSS of the individual genes. Direction of the arrow shows also whether the genes is transcribed on the + or – strand. B) Motif analysis identifies the (half-)binding motif for Zeb2 as CACCTG.

Figure S7. Gene-to-Disease association of the D8 DEGs bound by Zeb2.

The gene names of the DEGs expressed at D8 of neural differentiation were initially subjected to a mouse to human gene conversion. After that, gene to disease association analysis was performed showing that a number of those genes, could be associated with neurodevelopmental disorders, mental disorders, eye defects, seizures and speech impairment.

Supplementary Tables

Supplementary tables

Table S1: List of primers used in the study.

Primer name	Sense/Antisense	Sequence (5’ -> 3’)	Application
FlV5mZeb2Ex9_Fwd	Sense	GGCTTACCTGCAGAGCATCA	genotyping
FlV5mZeb2Ex9_Rev	Antisense	CTCCATCTAACTCTGTCTTGGC	genotyping
FlV5_Fwd	Sense	CTACTCGCAGCACATGAATC	genotyping
FlV5_Rev	Antisense	GAGAGGGTTAGGGATAGGC	genotyping
ΔZP_P1_Fwd	Sense	GTCAGTCCGTCCCCAGGTTT	genotyping
ΔZP_P2_Rev	Antisense	GGCATGCTAGCTGGGCTGGT	genotyping
LN249_Fwd	Sense	GGAGCAAACTGAACAAAACCTCGCC	genotyping
LN249_Rev	Antisense	GGCGAGGTTTTGTTCAGTTTGCTCC	genotyping
LN209_Fwd	Sense	AGCGGATCAGATGGCAGTTCGCATG	genotyping
LN209_Rev	Antisense	CATGCGAACTGCCATCTGATCCGCT	genotyping
Zeb2_Fwd	Sense	CAATGCAGCACTTAGGTGTA	qPCR
Zeb2_Rev	Antisense	TTGCCTAGAAACCGTATTGT	qPCR
Zeb2V5_Fwd	Sense	GAAACGATACGGGATGAGGA	qPCR
Zeb2V5_Rev	Antisense	AGGAGAGGGTTAGGGATAGG	qPCR
Nanog_Fwd	Sense	TCT TCC TGG TCC CCA CAG TTT	qPCR
Nanog_Rev	Antisense	GCA AGA ATA GTT CTC GGG ATG AA	qPCR
Pou5f1_Fwd	Sense	AGA GGA TCA CCT TGG GGT ACA	qPCR
Pou5f1_Rev	Antisense	CGA AGC GAC AGA TGG TGG TC	qPCR
Sox2_Fwd	Sense	GCGGAGTGGAAACTTTTGTCC	qPCR
Sox2_Rev	Antisense	CGGGAAGCGTGTACTTATCCTT	qPCR
Pax6_Fwd	Sense	ACATCTTTTACCCAAGAGCA	qPCR
Pax6_Rev	Antisense	GGCAAACACATCTGGATAAT	qPCR
Acrv1b_Fwd	Sense	CTGCCTACAGACCAACTACACC	qPCR

Acrv1b_Rev	Antisense	CCACGCCATCCAGGTTAAAGA	qPCR
Lhx5_Fwd	Sense	AGAACCGAAGGTCCAAAGAA	qPCR
Lhx5_Rev	Antisense	TCACTTTGGTAGTCTCCGTA	qPCR
Ntng2_Fwd	Sense	CAAGGACTCTACGCTTTTCG	qPCR
Ntng2_Rev	Antisense	AGCACTCGCAGTCTTGAAAT	qPCR
Sema3f_Fwd	Sense	CTACACAGCATCCTCCAAGA	qPCR
Sema3f_Rev	Antisense	ACGGCATTCTTGTTTGCATT	qPCR
Smad1_Fwd	Sense	TACTATGAGCTCAACAACCG	qPCR
Smad1_Rev	Antisense	GAAGCGGTTCTTATTGTTGG	qPCR
Smad3_Fwd	Sense	CACGCAGAACGTGAACACC	qPCR
Smad3_Rev	Antisense	GGCAGTAGATAACGTGAGGGA	qPCR
Sox13_Fwd	Sense	CTTACAGGAGGTTGTGCCA	qPCR
Sox13_Rev	Antisense	TCCTTAGCTTCCACATTGCT	qPCR
Stat3_Fwd	Sense	CAATACCATTGACCTGCCGAT	qPCR
Stat3_Rev	Antisense	GAGCGACTCAAACTGCCCT	qPCR
Tcf4_Fwd	Sense	TTGAAGATGTTTTCGCCTCC	qPCR
Tcf4_Rev	Antisense	CCTGCTAGTCATGTGGTCAT	qPCR
Tgfbr2_Fwd	Sense	GAAGGAAAAGAAAAGGGCGG	qPCR
Tgfbr2_Rev	Antisense	TGCTGGTGGTGTATTCTTCC	qPCR
Amylase_Fwd	Sense	GGCTGAGTGTTCTGGGAT	ChIP-qPCR
Amylase_Rev	Antisense	CACGGTGCTCTGGTAGAT	ChIP-qPCR
Cdh1_R1_Fwd	Sense	GCTAGGCTAGGATTCGAACGAC	ChIP-qPCR
Cdh1_R1_Rev	Antisense	TGCAGGGCCCTCAACTT	ChIP-qPCR

Table S2: shRNAs used.

Name	**Sequence**
shZeb2_1	CCGG**CCGAATGAGAAACAATATCAA**CTCGAGTTGATATTGTTTCTCATTCGGTTTTTG
shZeb2_2	CCGG**CCTCAGGAATTTGTGAAGGAA**CTCGAGTTCCTTCACAAATTCCTGAGGTTTTTG
shZeb2_3	CCGG**CCAGTGTCAGATTTGTAAGAA**CTCGAGTTCTTACAAATCTGACACTGGTTTTTG
shZeb2_4	CCGG**CCCATTTAGTGCCAAGCCTTT**CTCGAGAAAGGCTTGGCACTAAATGGGTTTTTG
shCTRL	CCGGCAACAAGATGAAGAGCACCAACTCGAGTTGGTGCTCTTCATCTTGTTGTTTTT

Supplementary Files

File S1. Narrow peaks obtained from the ChIP-seq.

File S2. Transcriptomic data of Zeb2 bound genes in differentiating mESCs.

File S3. Target genes bound by Zeb2 and deregulated in different already published RNA-seq datasets.

Abbreviations

bHLH: basic helix-loop-helix
BMP: bone morphogenetic protein
ChIP: chromatin immunoprecipitation
CNS: central nervous system
D: day
DEG: differentially expressed gene
EMT: epithelial-to-mesenchymal transition
EpiLSC: epiblast stem cell like cell
ESC: embryonic stem cell
esiRNA: endoribonuclease-generated interfering RNA
ex: exon
GFP: green fluorescent protein
GO: gene ontology
gRNA: guide RNA
GWBS: genome-wide binding sites
KD: knockdown
KO: knockout
lncRNA: long non-coding RNA
miR: micro-RNA
MOWS: Mowat-Wilson syndrome
ND: neurodifferentiation
NPC: neuroprogenitor\
OPC: oligodendrocyte precursor
PTHS: Pitt-Hopkins syndrome
RNA-seq: RNA- sequencing
RT: room temperature
RT-qPCR: reverse transcription quantitative polymerase chain reaction
shRNA: short-hairpin RNA
TF: transcription factor
TGFβ: transforming growth factor type β
TSS: transcription start site
V-SVZ: ventricular-subventricular zone

Figure 1

A

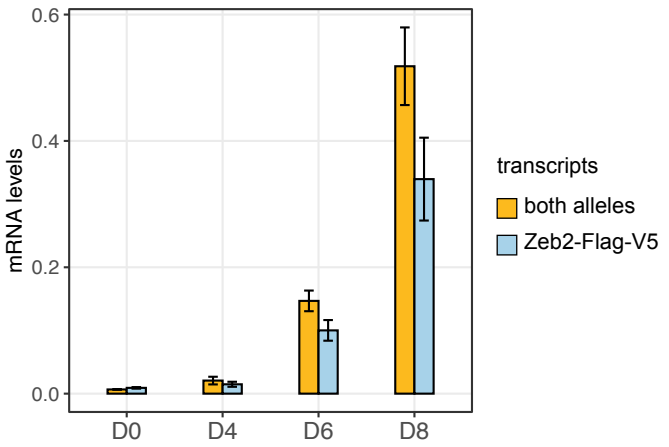

B

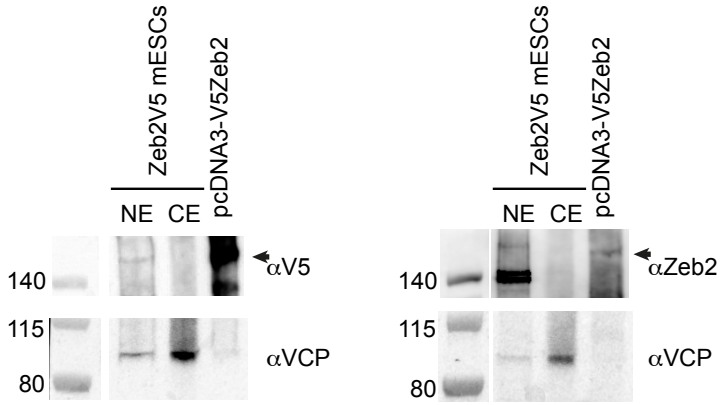

C

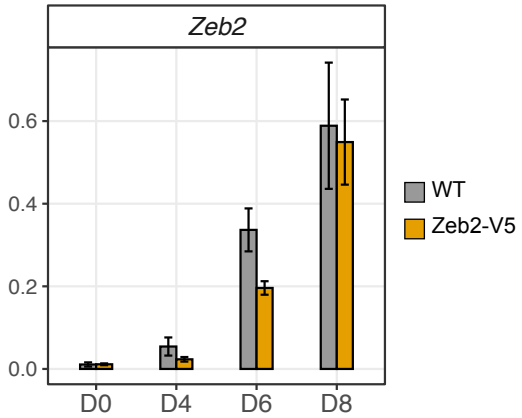

D

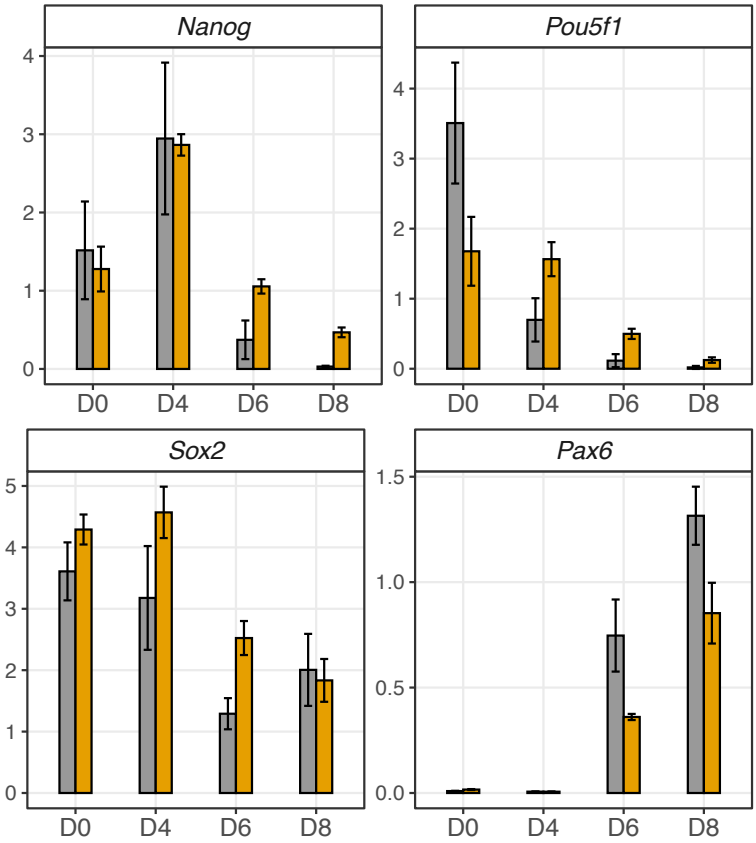

E

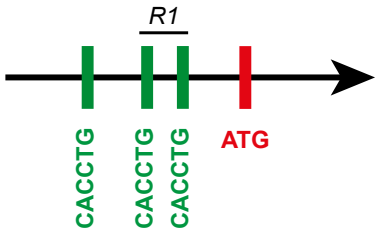

F

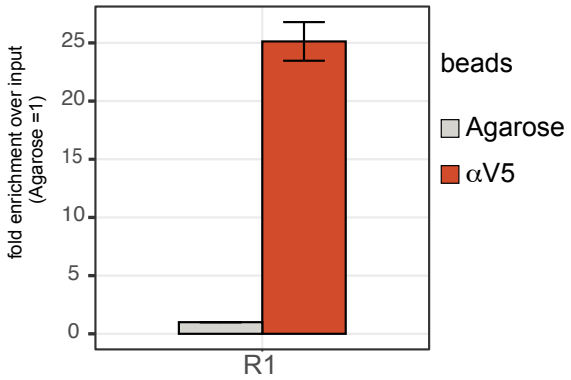

Figure 2

A

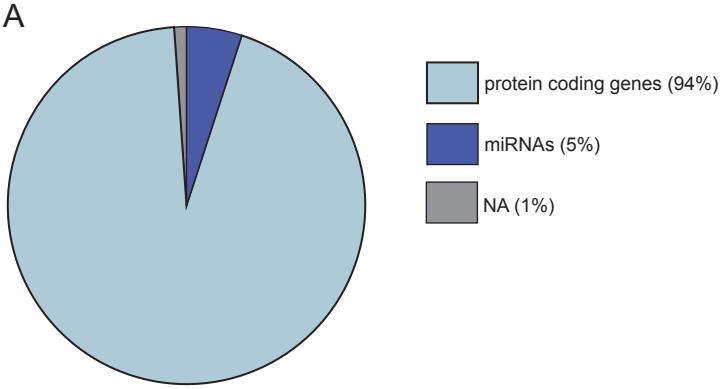

B

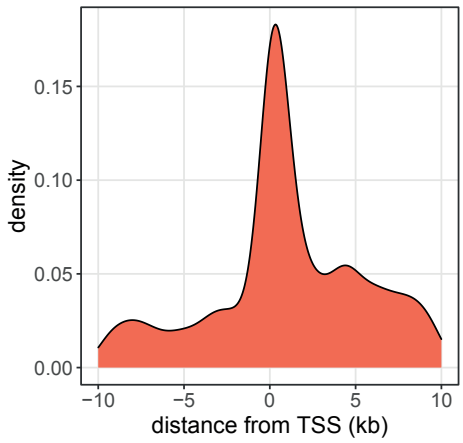

C

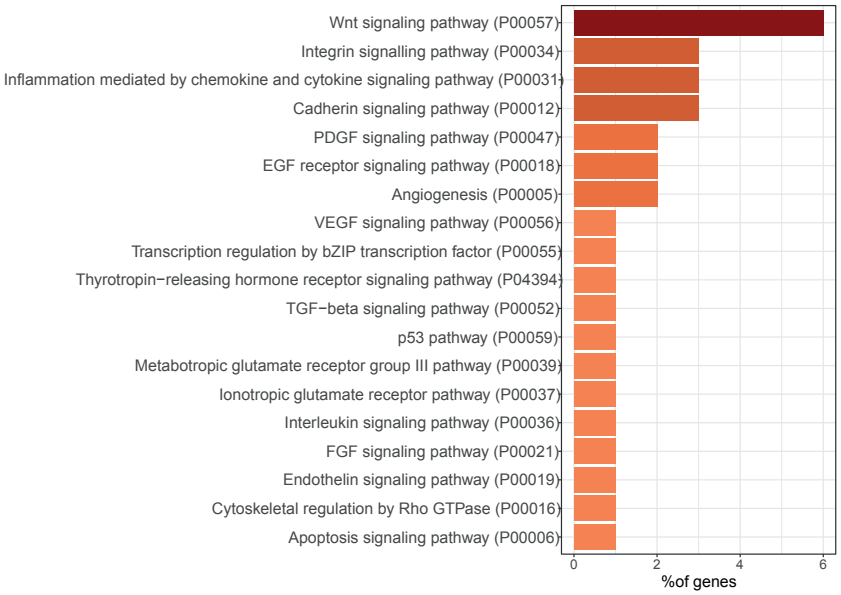

D

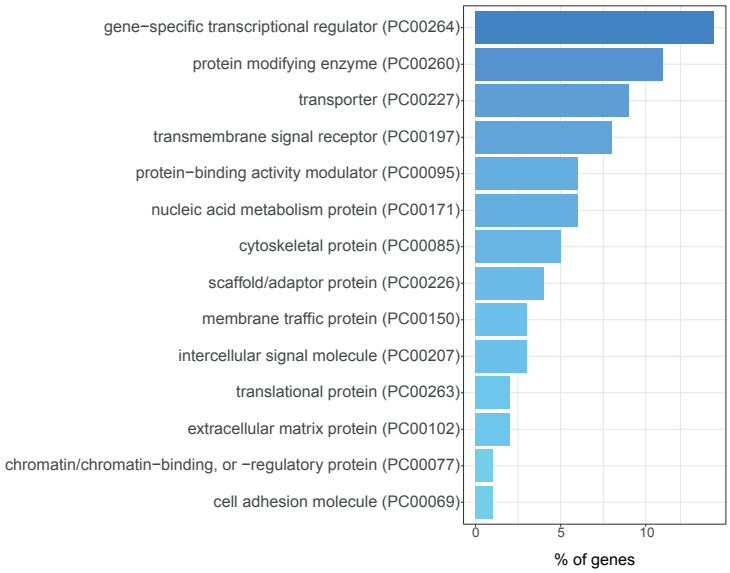

E

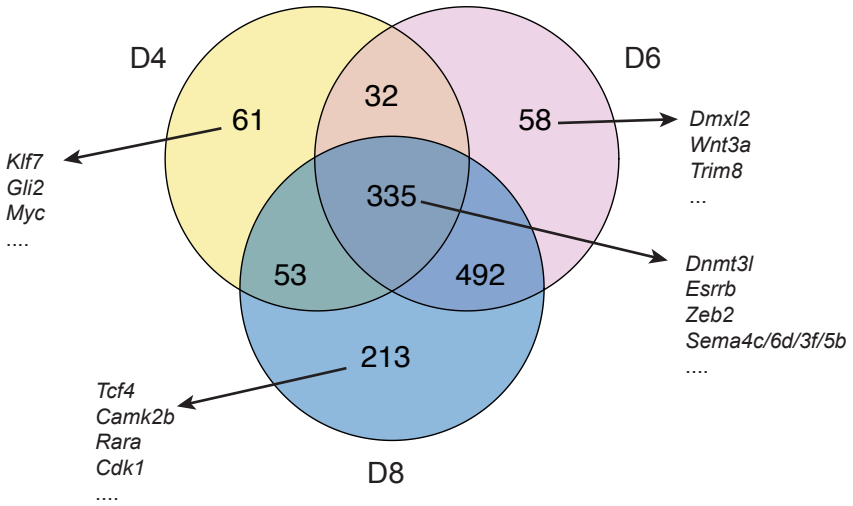

	up	down
D4	297	184
D6	523	394
D8	612	481

F

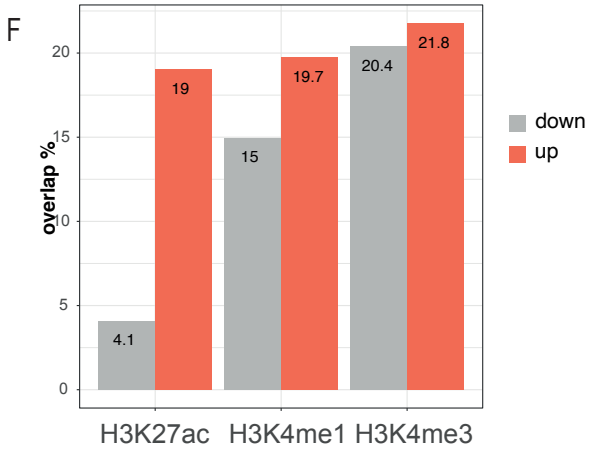

G

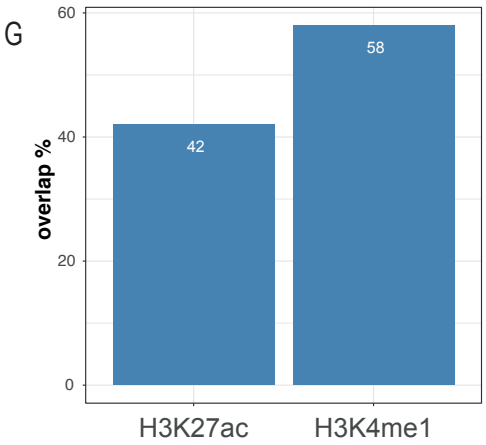

Figure 3

A

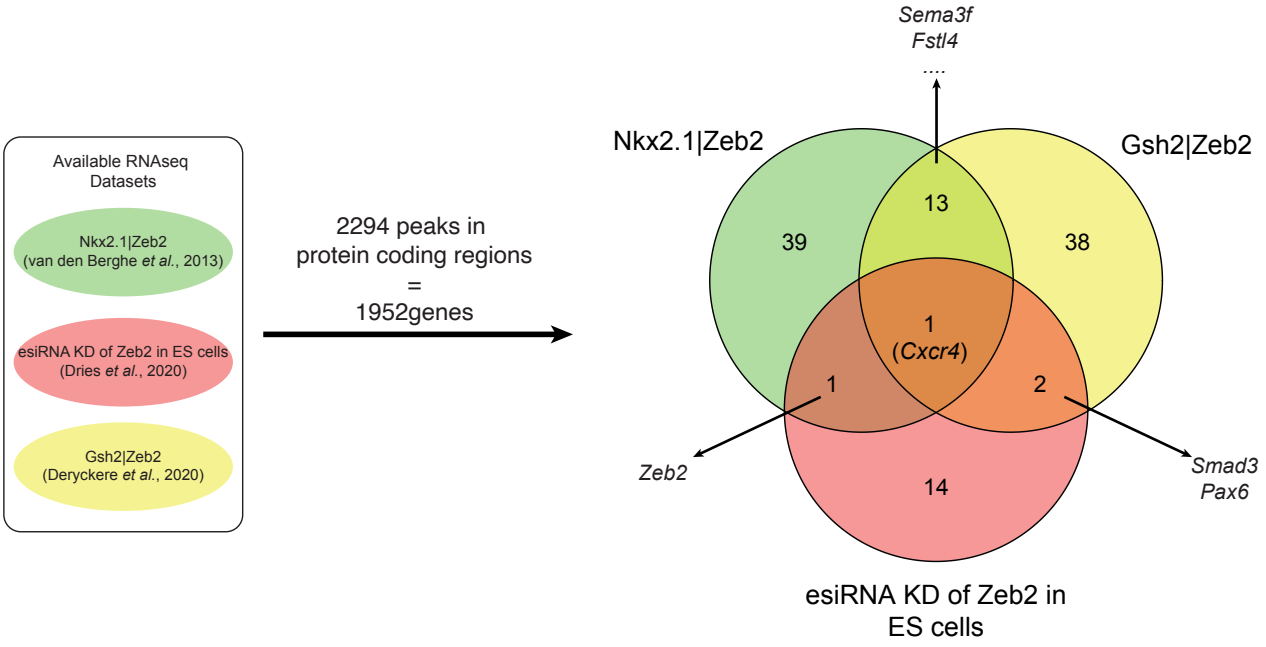
Available RNAseq Datasets
Nkx2.1|Zeb2 (van den Berghe et al., 2013)
esiRNA KD of Zeb2 in ES cells (Dries et al., 2020)
Gsh2|Zeb2 (Deryckere et al., 2020)
2294 peaks in protein coding regions = 1952genes
Sema3f
Fstl4
....
Nkx2.1|Zeb2
Gsh2|Zeb2
39
13
38
1 (Cxcr4)
1
2
14
Zeb2
Smad3
Pax6
esiRNA KD of Zeb2 in ES cells

B

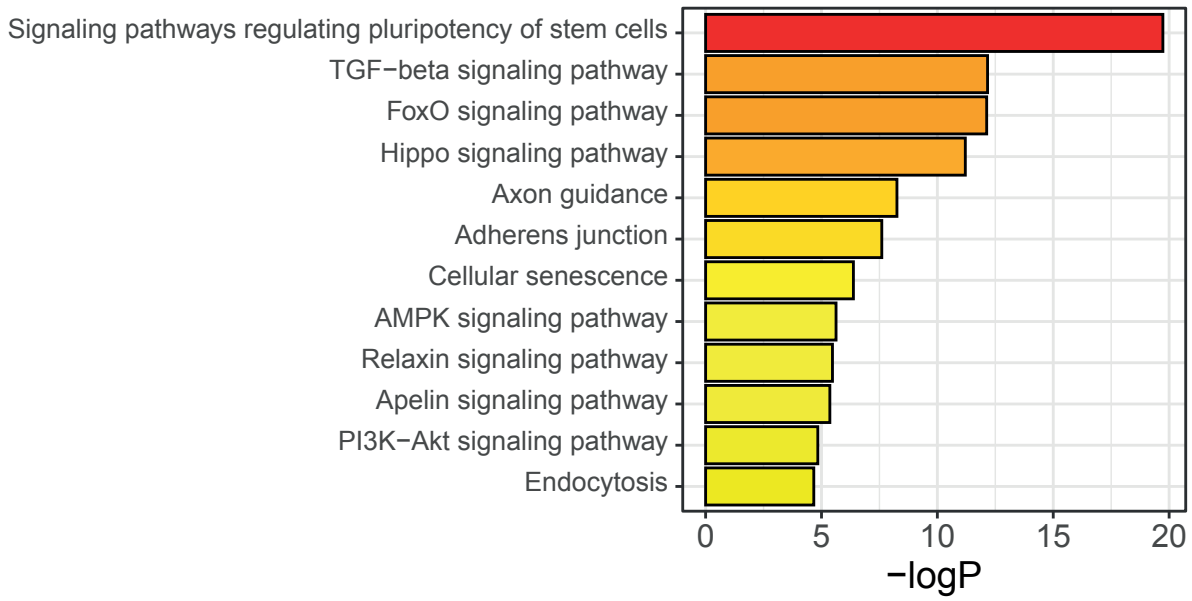
Signaling pathways regulating pluripotency of stem cells
TGF−beta signaling pathway
FoxO signaling pathway
Hippo signaling pathway
Axon guidance
Adherens junction
Cellular senescence
AMPK signaling pathway
Relaxin signaling pathway
Apelin signaling pathway
PI3K−Akt signaling pathway
Endocytosis
0
5
10
15
20
−logP

Figure 4

A

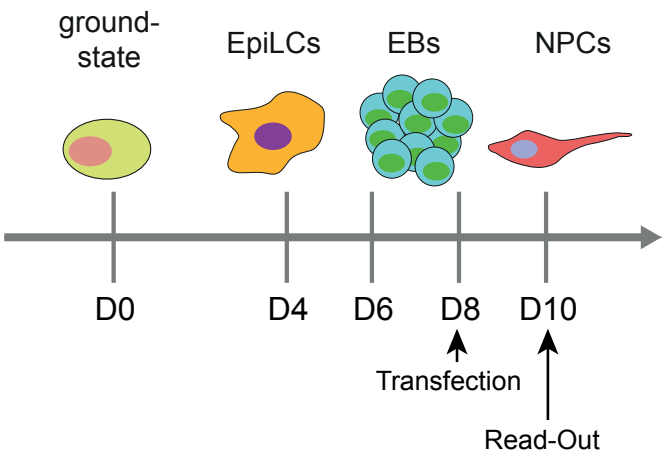
ground-state
EpiLCs
EBs
NPCs
D0
D4
D6
D8
D10
Transfection
Read-Out

B

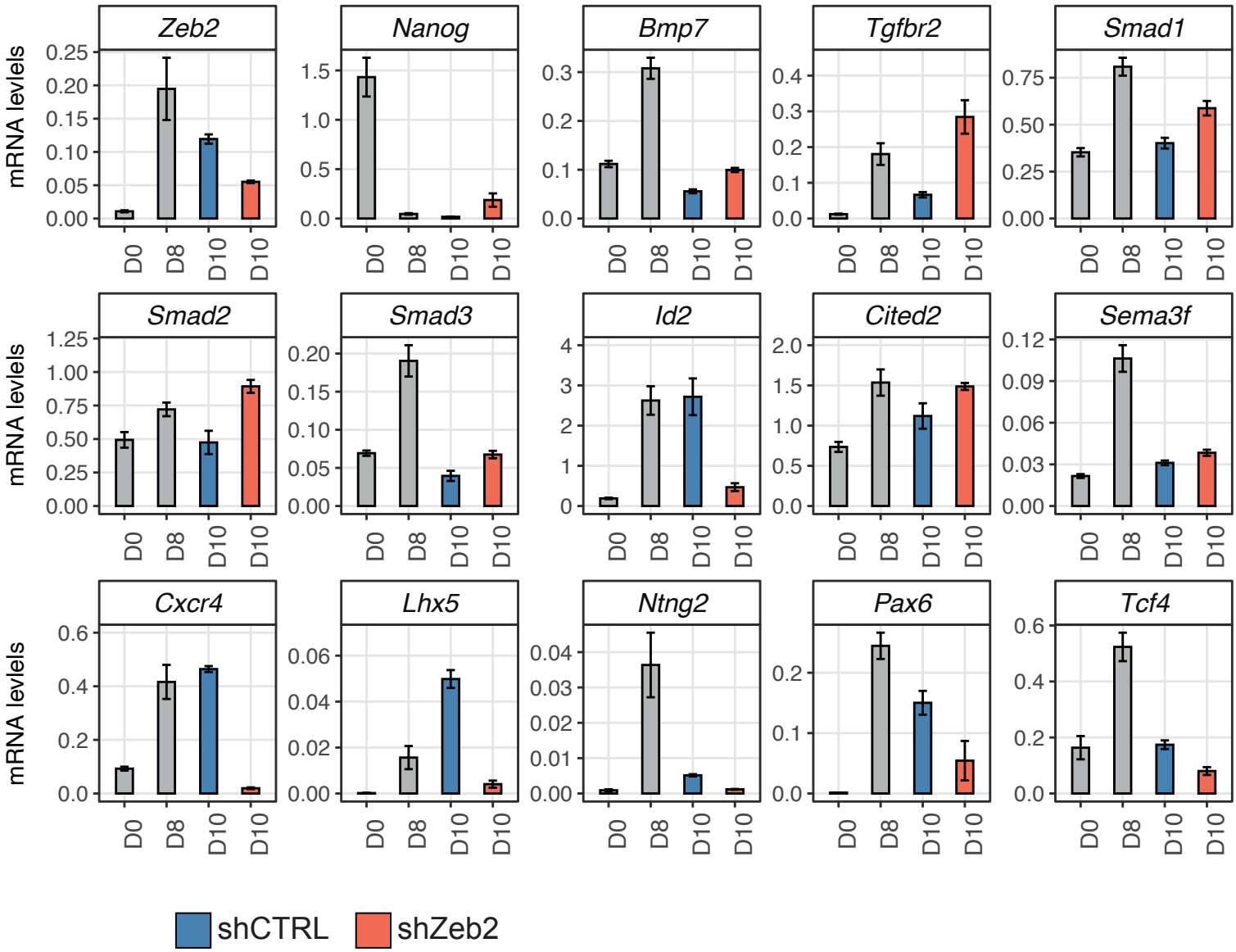
Zeb2
Nanog
Bmp7
Tgfbr2
Smad1
Smad2
Smad3
Id2
Cited2
Sema3f
Cxcr4
Lhx5
Ntng2
Pax6
Tcf4
mRNA levels
D0
D8
D10
D10
shCTRL
shZeb2

Figure 5

A

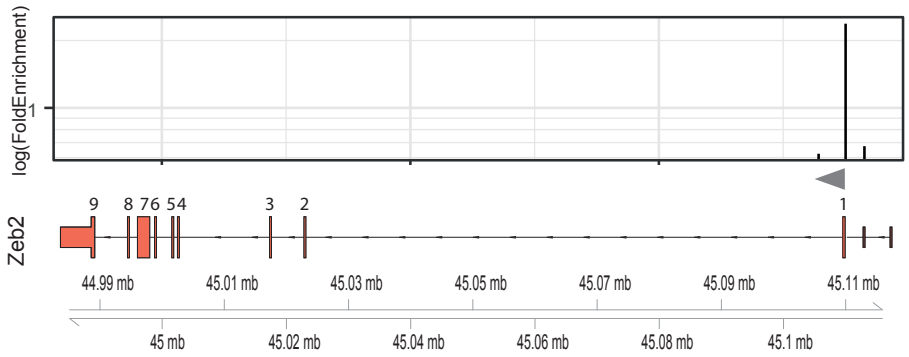
log(FoldEnrichment)
1
Zeb2
9
8 76 54
3
2
1
44.99 mb
45.01 mb
45.03 mb
45.05 mb
45.07 mb
45.09 mb
45.11 mb
45 mb
45.02 mb
45.04 mb
45.06 mb
45.08 mb
45.1 mb

B

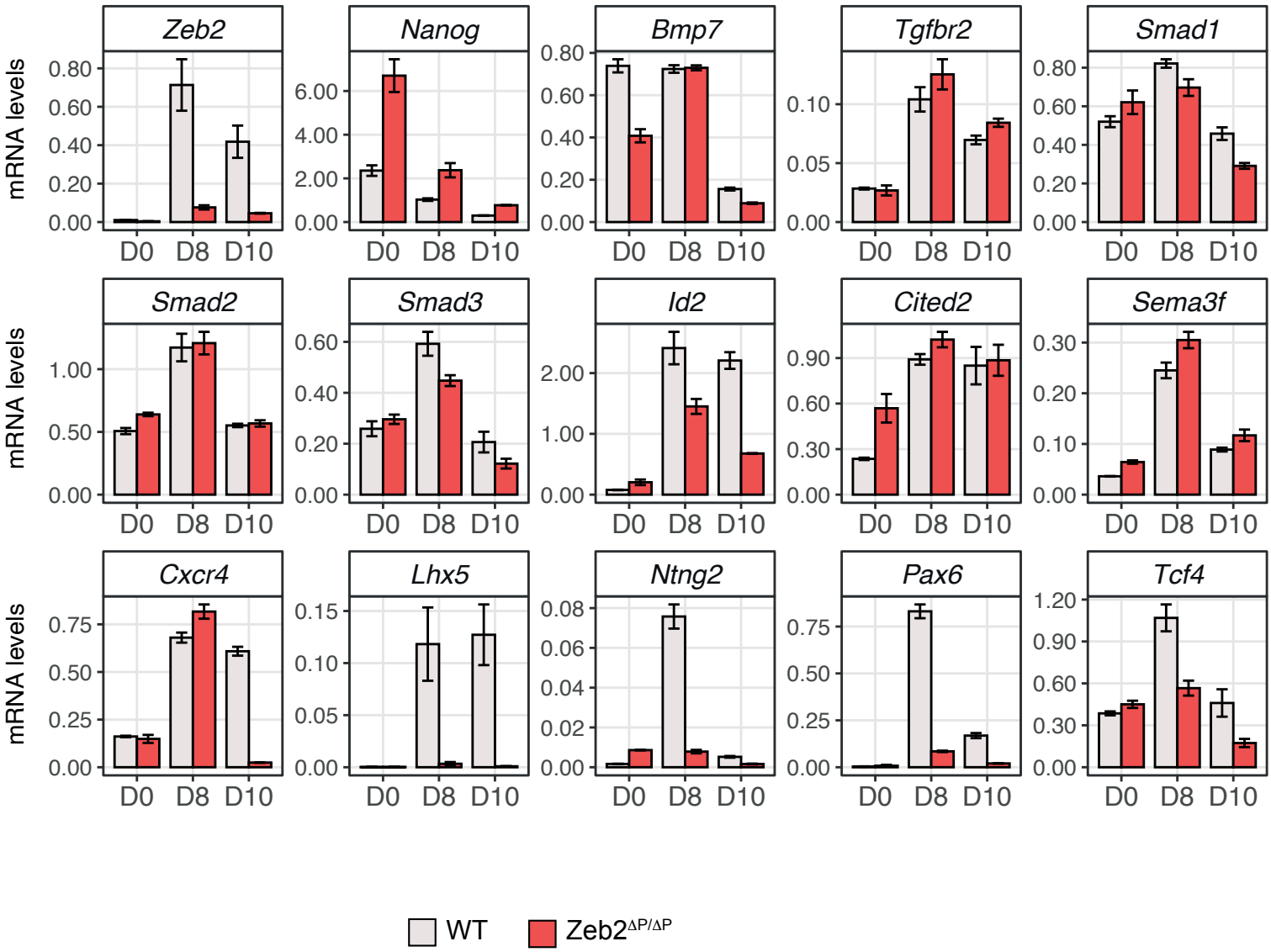
Zeb2
Nanog
Bmp7
Tgfbr2
Smad1
Smad2
Smad3
Id2
Cited2
Sema3f
Cxcr4
Lhx5
Ntng2
Pax6
Tcf4
mRNA levels
D0
D8
D10
WT
Zeb2ΔP/ΔP